IDENTIFICATION OF DYNAMIC FOUNDATION STIFFNESSES AND INPUT MOTIONS FROM STRONG MOTION DATA RECORDED AT CSMIP INSTRUMENTED BUILDINGS

S.F. Ghahari and E. Taciroglu

Department of Civil & Environmental Engineering

University of California, Los Angeles

Abstract

Substructure method is commonly used in engineering practice to take Soil-Structure Interaction (SSI) effects into account in seismic design. In this method, soil is modeled using discrete spring elements—ideally Impedance Functions (IF)—that are attached to the superstructure; and the Foundation Input Motions (FIMs) are applied at the remote ends of these springs. While the application of the substructure method is simple and its computational cost is low, the determination of FIMs and the IFs are generally challenging. This paper presents results of a two-year project during which a new method was developed to identify IFs and to back-calculate FIMs from earthquake data recorded at CSMIP-instrumented buildings. The method features a flexible-based Timoshenko beam idealization of the superstructure and its soil-foundation system, and is based on updating the parameters of this model such that its responses match real-life data. Details of the said method are briefly reviewed first, followed by a presentation of the results it produced on currently available CSMIP data.

Introduction

Soil-Structure Interaction (SSI) has been a research subject for more than 40 years (Jennings & Kuroiwa, 1968; Richat, 1975; Wolf, 1976). SSI effects can be classified into two distinct effects: *kinematic* and *inertial* (Wolf & Deeks, 2004). Dubbed the Foundation Input Motions (FIMs), the earthquake excitations experienced by a structure-foundation system are altered by the foundation stiffness and distinct geometry. Therefore, FIMs are generally different from the Free-Field Motions (FFMs) that would have been recorded in the absence of the foundation. The effects causing the said differences in FIMs and FFMs are collectively referred to as kinematic effects. Inertial interaction effects are due to the mass of the foundation-superstructure system, which imparts inertial forces onto the surrounding soil and causes the foundation to experience a response that is different from the FIM. Due to inertial effects, the vibrating structure operates as a wave source and alters the wave field around the foundation system (Abrahamson et al., 1991).

The direct and the substructure methods are two approaches used for taking SSI effects into account in seismic response analyses. In the direct method, a complete—usually a Finite Element (FE)—model of the soil-structure system is created wherein the soil medium is represented as a semi-infinite domain (Pak & Guzina, 1999; Rizos & Wang, 2002). Due to its labor-intensive model development and high computational costs, the direct method is typically avoided in engineering practice. In the substructure method, the SSI problem is typically

decomposed into three distinct parts (Stewart et al., 1998): (*i*) estimation of FIMs, (*ii*) determination of the frequency-dependent soil-foundation Impedance Functions (IFs), and (*iii*) dynamic analysis of the super-structure supported on a compliant base represented by the IFs and subjected to the FIMs.

Accurate estimation of FIMs and IFs control the accuracy of the substructure method. However, available formulations for estimation/determination of FIMs and IFs are primarily limited to analytical studies (Gazetas, 1983; Iguchi & Luco, 1981; Çelebi et al., 2006), which are typically confined to simple foundation geometry and soil conditions, or experimental data with relatively low-amplitude excitations (Tileylioglu et al., 2010). Motivated by this, the present project's aim has been to develop a robust, accurate, and broadly applicable method to identify IFs and FIMs from earthquake-induced response signals recorded on instrumented buildings. Using real-life data is key, because neither field (e.g., forced vibration) nor laboratory (e.g., centrifuge) tests can mimic the range of complexities encountered in the field—the former cannot induce strong motion amplitudes at broad frequency bands, and the latter cannot provide the full set of complexities of soil constitutive behavior or wave propagation patterns.

The method devised in the present effort is based on representing the superstructure-foundation-soil systems through flexible-base Timoshenko beam models, and subsequently estimating models parameters (i.e., soil-foundation IFs and Timoshenko beam properties) by minimizing the discrepancy between the model-predicted and real-life dynamics responses.

The simplified model adopted in the present study (i.e., the flexible-base Timoshenko) nominally precludes the investigation of the frequency-dependency of the foundation system of a single building. However, because the devised identification method was applied to a large set of buildings here, it produced results that illuminate the behavior of several classes of foundation systems at a range of excitation frequencies. This study involved analyses of 373 earthquake datasets from 21 steel and 40 concrete instrumented buildings of the California Strong Motion Instrumentation Program (CSMIP) (see, Huang and Shakal, 2001). These records were judiciously selected from the current CSMIP building inventory using a Matlab-based (Matlab, 2013) data classification toolbox named CSMIP-CIT that was developed for the present project, into which the developed identification method is also implemented (Ghahari et al., 2015).

As the basic formulation, verification, and application of the developed identification method to a particular case—namely, the Millikan Library in Pasadena CA were previously presented (Taciroglu et al., 2016a and b)—, only a brief overview of the method is provided in what follows. The remainder of the manuscript is devoted to the presentation of the selected data, the results obtained from those data, and finally a discussion of findings in comparison to previous key studies on SSI.

The Proposed Identification Method

Consider a Timoshenko beam (1921) resting on a sway-rocking foundation as shown in Figure 1. Through modal superposition, the absolute acceleration of the beam under horizontal base acceleration—i.e., $\ddot{u}_g(t)$, which can be a real-life recording—, can be written as

$$\ddot{y}^t(x,t) = \sum_{j=1}^{n} W_j(x)\ddot{q}_j(t) \;\; + \ddot{u}_g(t) \tag{1}$$

where $\ddot{q}_j(t)$ is relative acceleration of a SDOF system under $\beta_j \ddot{u}_g(t)$ with β_j being the modal contribution factor. $W_j(x)$ is a function that describes the *j*-th normal mode shape for lateral displacements, and can be obtained via modal analysis of the model as described in (Taciroglu et al., 2016a). This function has 5 dimensionless parameters; namely,

$$s^2 = \frac{EI}{GA_sL^2}, \quad b_j^2 = \frac{\rho A {\omega_j}^2 L^4}{EI}, \; k_T = \frac{K_T}{GA_s/L}, \quad k_R = \frac{K_R}{EI/L} \quad R^2 = \frac{I}{AL^2} \tag{2}$$

where E, G, ρ, and A are the Young's and shear moduli, mass density, and section area, respectively. To consider the non-uniform distribution of shear stress within the Timoshenko beam's cross-section, $A_s = \kappa A$ is used as the effective shear cross-sectional area, where κ can be approximated as 0.85 for rectangular sections (Cowper, 1966). ω_j is the *j*-th natural frequency, and K_T and K_R are the nominally frequency-dependent soil-foundation stiffnesses, which are assumed to be frequency independent in the proposed method for simplicity. To calculate the modal coordinates ($\ddot{q}_j(t)$), modal orthogonality with respect to mass matrix (**M**) can be used (Han et al., 1999). Hence, $q_j(t)$, and consequently its time derivatives, can be identified from the equation below

$$\ddot{q}_j(t) + {\omega_j}^2 \, q_j(t) = \beta_j \ddot{u}_g(t) \tag{3}$$

where the modal contribution factor is $\beta_j = L_j^*/m_j^*$. Here L_j^* and m_j^* denote, respectively, the generalized influence factor and mass, and are defined as

$$L_j^* = \rho A \int_0^L W_j(x)\, dx \;, \quad m_j^* = \int_0^L \boldsymbol{\varphi}_j(x)^T \, \mathbf{M} \, \boldsymbol{\varphi}_j(x) \tag{4}$$

where

$$\boldsymbol{\varphi}_j(x) = \begin{bmatrix} W_j(x) \\ \Theta_j(x) \end{bmatrix} \tag{5}$$

where $\Theta_j(x)$ is a function describing the *j*-th normal mode shape for rotational deformations. To consider damping, while retaining the normal-mode assumption, we add a term $2\,\omega_j\,\xi_j\,\dot{q}_j(t)$ with ξ_j being the *j*-th modal damping ratio to Eq. (3), to make it similar to the response of a damped SDOF system (Chopra, 2001).

For the proposed identification method, we assume that the absolute acceleration of a flexible-base building is available at three levels—namely, the foundation level $\ddot{y}^t(0,t)$, the mid-height level $\ddot{y}^t(x_m,t)$, and the roof $\ddot{y}^t(L,t)$. According to Eqs. (1) and (3), each of these response signals can be expressed in the frequency domain as

$$\ddot{y}^t(x,\omega) = \left[\sum_{j=1}^{n} W_j(x)\,\beta_j H_j(\omega) + 1\right] \ddot{u}_g(\omega) \tag{6}$$

with

$$H_j(\omega) = \frac{-\omega^2}{{\omega_j}^2 - \omega^2 + 2i\xi_j\omega_j\omega}. \tag{7}$$

Accordingly, the response at mid-height and the roof can be predicted by the response of the foundation level by eliminating the input excitation as in

$$\ddot{y}^t(x,\omega) = \frac{\left[\sum_{j=1}^{n} W_j(x)\,\beta_j H_j(\omega) + 1\right]}{\left[\sum_{j=1}^{n} W_j(0)\,\beta_j H_j(\omega) + 1\right]} \ddot{y}^t(0,\omega). \tag{8}$$

Therefore, by defining and solving a proper minimization problem, the unknown parameters of the system can be identified. A similar approach has been successfully used by Lignos and Miranda (2014) to identify the input motion of fixed-base structures, who linked shear and flexural beams to represent their parametric models.

We define the following optimization problem here

$$\min_{\bar{b},s,k_T,k_R,\xi_1,\ldots,\xi_n} \left\|\ddot{y}^t(x_m,t) - \ddot{\tilde{y}}^t(x_m,t)\right\| + \left\|\ddot{y}^t(L,t) - \ddot{\tilde{y}}^t(L,t)\right\| \tag{9}$$

where $\ddot{\tilde{y}}^t(x_m,t)$ and $\ddot{\tilde{y}}^t(L,t)$ denote the response signals recorded at mid-height and roof levels, respectively, and $\ddot{y}^t(x_m,t)$ and $\ddot{y}^t(L,t)$ are their counterparts predicted by Eq. (8) and transformed to the time domain through Inverse Fourier Transform. We replace the dimensionless parameter b_j with $\bar{b} = b_j/\omega_j$ to make it mode-independent. This optimization problem is non-convex and may have several local minima. We, therefore devise constraints to decrease the possibility of being trapped in a local minimum. As the first flexible-base natural frequency can be easily detected from the Fourier spectrum of the roof response using simple peak-picking, we add this information as a constraint to the optimization problem. Moreover, we start the optimization procedure with multiple random starting points.

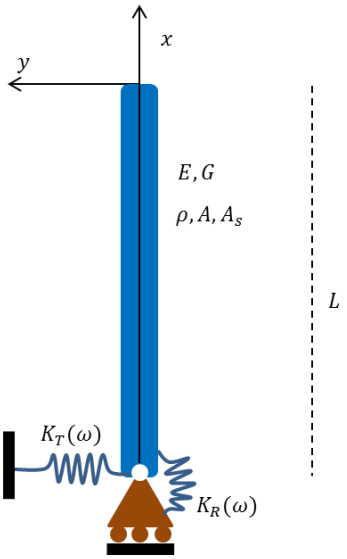

Figure 1. Timoshenko beam model of a soil-structure system.

Once the unknown parameters are identified by solving the optimization problem, the unknown input motion, $\ddot{u}_g(\omega)$, can be back-calculated through Eq. (6) using any of the available measured response signals. Additionally, the foundation rocking response can be estimated by converting the foundation translational response, as in

$$\ddot{\alpha}(x,\omega) = \frac{\left[\sum_{j=1}^{n} \Theta_j(0)\,\beta_j H_j(\omega)\right]}{\left[\sum_{j=1}^{n} W_j(0)\,\beta_j H_j(\omega) + 1\right]}\,\ddot{y}^t(0,\omega) \tag{10}$$

To identify the pseudo-flexible and fixed base damping ratios (Stewart & Fenves, 1998), we can easily define optimization problems similar to Eq. (9).

For the pseudo-flexible model, we can predict the response of mid-height and roof levels by analyzing a pseudo-flexible base Timoshenko beam subjected to horizontal foundation response, using Eq. (6). In this case, all modal properties—i.e., ω_j, ξ_j, m_j^*, L_j^*, and $W_j(x)$—must be calculated for a pseudo-flexible Timoshenko beam, while $\ddot{u}_g(\omega)$ must be $\ddot{y}^t(0,\omega)$. The damping ratio is then identified by solving a minimization problem such that the predicted mid-height and roof level responses match the recorded responses.

For the fixed-flexible model, we can predict the response at mid-height and roof levels by analyzing a fixed-base Timoshenko beam subjected to horizontal and rocking foundation responses, and by minimizing the difference between predicted and recorded signals. Note that the foundation-rocking response is already predicted through Eq. (10). To predict the response of a fixed-base Timoshenko beam model under horizontal ($\ddot{u}_g(\omega)$) and rocking ($\ddot{\theta}_g(\omega)$) base excitations, we have

$$\ddot{y}^t(x,\omega) = \left[\sum_{j=1}^{n} W_j(x)\,\beta_j H_j(\omega) + 1\right]\ddot{u}_g(\omega) + \left[\sum_{j=1}^{n} W_j(x)\,\bar{\beta}_j H_j(\omega) + x\right]\ddot{\theta}_g(\omega) \tag{11}$$

where again $\beta_j = L_j^*/m_j^*$ and $\bar{\beta}_j = \bar{L}_j^*/m_j^*$. The terms L_j^* and m_j^* are calculated using Eq. (4), and $H_j(\omega)$ is calculated using Eq. (7) wherein the fixed-base mode shapes and natural frequencies must be used. $\bar{L}_j^*$ is the generalized influence factor for rocking excitation and must be calculated as in

$$\bar{L}_j^* = \rho\, I \int_0^L \Theta_j(x)\, dx + \rho\, A \int_0^L x\, W_j(x)\, dx \qquad 12)$$

using the fixed-base mode shapes.

Studied Data

CSMIP Database

Established in 1972, the California Strong Motion Instrumentation Program (CSMIP) aims to collect seismic response data from ground stations as well as representative structures (bridges, dams, and buildings). At the present time, there are more than 900 stations (650+ ground-response stations, 170+ buildings, 20 dams, and 60+ bridges). CSMIP stations are configured to collect data, when triggered by a seismic event, and the resulting records are archived for public use in searchable database—*viz.*, the Center for Engineering Strong Motion Database (CESMD)[1].

Data Classification

CESMD provides station metadata in addition to seismic recordings. These metadata enable the classification of building stations into sub-categories. Nevertheless, CESMD only offers basic search and sorting capabilities. Motivated by the need to look at behavior across different types (structural systems, foundation systems, and heights), we developed the CSMIP-CIT toolbox (as briefly described above), which automatically harvests the response data and station metadata, enables user-guided classification, and applies the identification method presented above (Ghahari et al 2015). This toolbox features a graphical user interface (Figure 2), and is able automatically generate a short report (Figure 3).

We employ the classification capability of CSMIP-CIT and processed the available data in CESMD[2]. Table 1 displays a summary of available *building* data. As seen, there are currently 377 instrumented buildings in CESMD (a complete list can be found in Taciroglu et al., 2016c). It is expedient to note here that only the data collected by California Geological Survey (CGS) was used in the present study, primarily out of necessity, because the channel numbers in both the instrumentation layout plans and the data files are identical only in the CGS data. As it can be seen from Figure 4, less than 70% of the buildings are instrumented by the CGS, which is equivalent to 259 buildings. Out of all 259 buildings instrumented by CGS, data from only 216 buildings are useable at the present time, due to the availability of both earthquake data and the instrumentation layouts (Table 2).

[1] www.strongmotioncenter.org

[2] The CSMIP-CIT database was last updated on 03/28/2016.

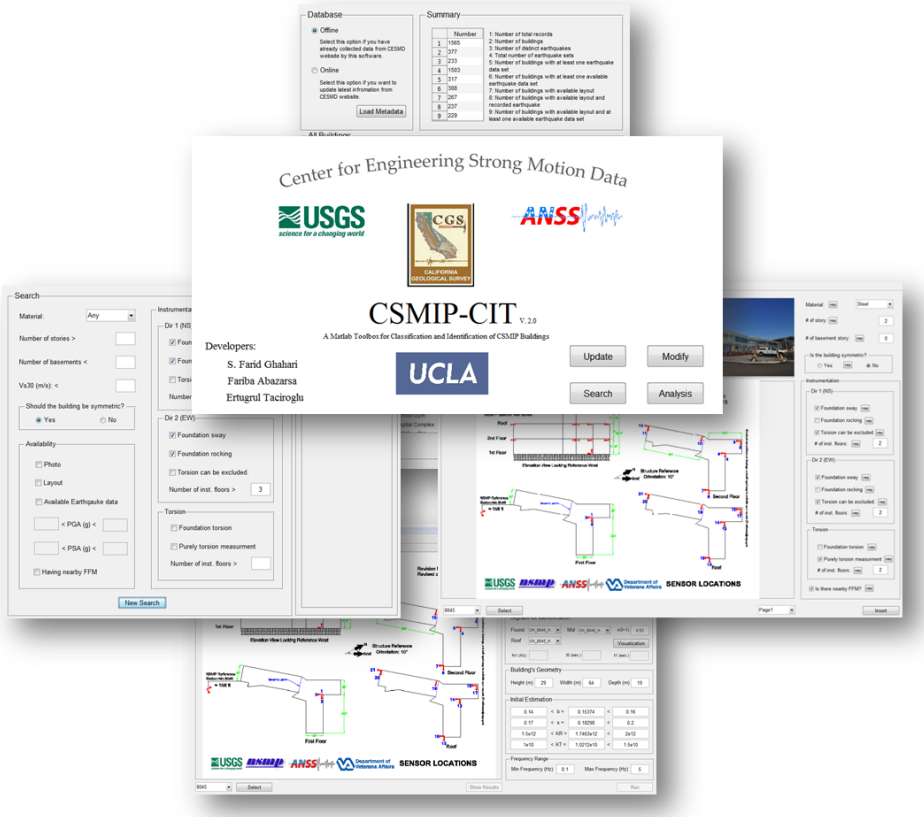

Figure 2. Graphical user interface of the CSMIP-CIT software.

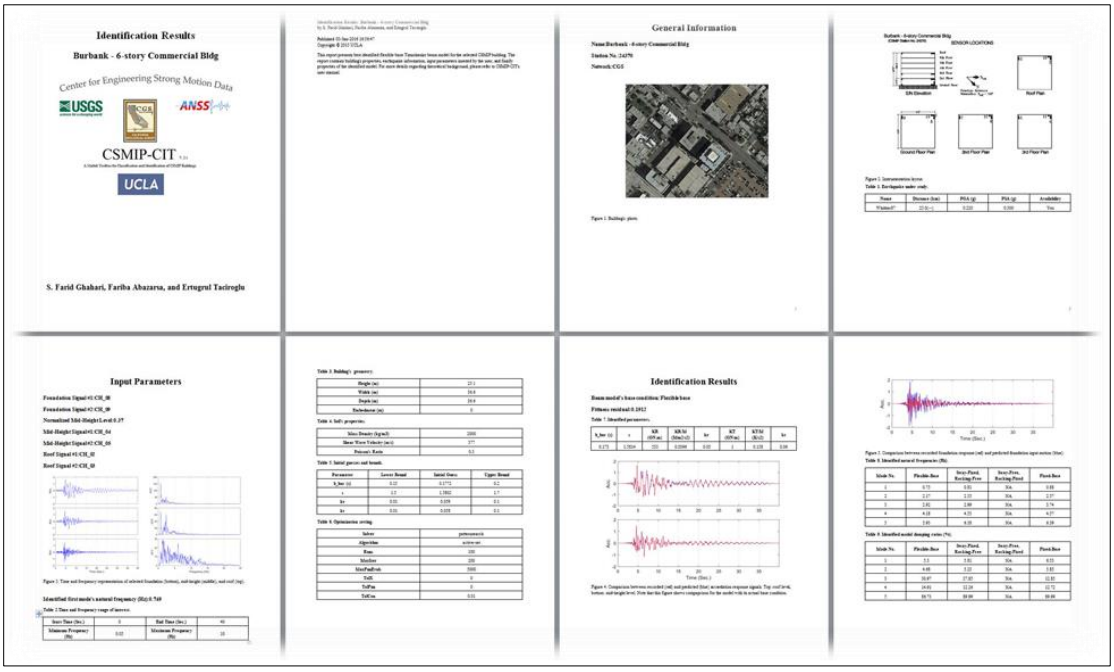

Figure 3. Report automatically generated by CSMIP-CIT software.

Table 1. Available building data in CESMD.

Item Description	Number
Number of total records	1643
Number of buildings	377
Number of earthquakes	254
Number of earthquae sets	1588
Number of buildings with at least one earthquake	322
Number of buildings with at least one available earthquake	314
Number of buildings with available layout	272
Number of buildings with available layout and at least one recorded earthquake	243
Number of buildings with available layout and at least one available earthquake	236

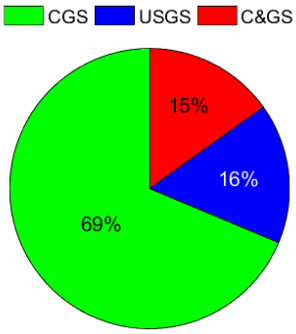

Figure 4. Distribution of the available data.

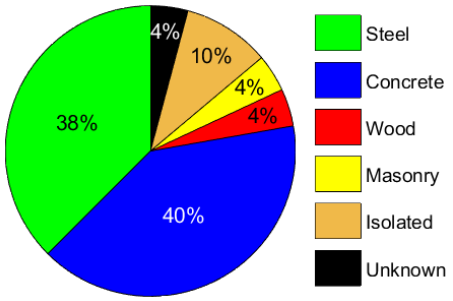

Figure 5. Materials of all 216 useable CGS buildings.

Table 2. Available building data in CESMD instrumented by CGS.

Item Description	Number
Number of buildings	259
Number of buildings with at least one available earthquake	218
Number of buildings with available layout	242
Number of buildings with available layout and at least one available earthquake	216

In the present study, we study only steel and concrete ordinary buildings (i.e., wood, masonry, and base isolation structures were excluded). Figure 5 indicates that ~80% of the 216 instrumented buildings are potentially subject of the present study, which are 168 buildings. Note that "Unknown" category in Figure 5 denotes those buildings whose lateral system could not be identified from their layout or description provided at CESMD.

It is well accepted that the identification of buildings from their earthquake-induced response signals is directly affected by the number and distribution of the sensors. Theoretically, soil-foundation flexibilities can be identified by investigating the difference between the so-called flexible-based and fixed-base system's properties (Stewart & Fenves, 1998). To identify both the fixed- and flexible-base properties, the FFM, foundation sway, foundation rocking, and building responses must be measured. However, the number of CSMIP buildings with necessary instrumentation for this purpose is very limited. As shown in Figure 6, under

Case 1, out of the 168 selected buildings, the total number of steel and concrete buildings that have instrumentation layouts, available earthquake records, nearby Free-Field Motion (FFM) stations, foundation sway and rocking instrumentations, and at least one instrumented floor is less than 10. It is useful to note that it may be possible to find FFM stations close to some of other buildings, but the aforementioned classification is based on FFM stations shown on the instrumentation layouts available in CESMD.

If we can relax the FFM requirement, then the number of buildings increases to 23 (denoted as Case 2). Such a number is still very small and cannot be used to extract aggregate results from which broad conclusions can be drawn. Another critical limitation is the availability of the foundation rocking measurement. The identification method devised in the present project is, therefore, a key tool, because with this method, it is now possible to quantify soil-structure interaction effects *even without foundation rocking measurements*. By relaxing the rocking measurement condition, the number of available buildings increases from 23 to around 164 (denoted as Case 3). Having only one sensor on the structure may not be able to capture contribution of different modes. Therefore, it is more favorable to have additional sensors, as used in Eq. (9). As the figure shows, by adding one more sensor as an additional requirement (denoted as Case 4), the number of buildings available for the study decreases, but not significantly (~129) [3]. Based on this fact, we designed CSMIP-CIT only for Case 4, through which 129 buildings can be analyzed at the present time.

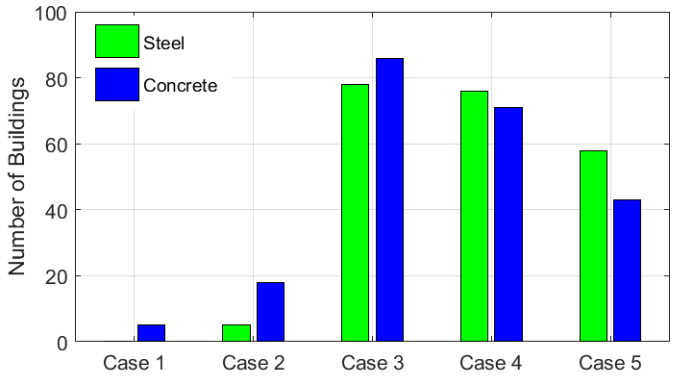

Figure 6. Number of instrumented buildings for various instrumentation scenarios.

Finally, because the current version of our identification method (and consequently CSMIP-CIT) is developed only for two-dimensional (2D) problems, we have to select those buildings whose two perpendicular directions are torsionally uncoupled. According to the available layouts, and based on the sensor locations and the distributions of mass and stiffness, we concluded that there are 44 steel and 58 concrete (a total of 102) buildings in the database whose data can be analyzed by the current version of CSMIP-CIT. A complete list of these candidate buildings is presented in Table A (of Appendix A). In this table, it is indicated—by using "Y" (yes) and "N" (no)—whether the instrumentation deployment is capable or incapable to measure 2D responses of the building in each direction. The table also provides the types of lateral structural system in each direction (for those having suitable sensor deployments). Note that a "+" sign indicates that several structural systems work in parallel, while the moniker

[3] Requiring one additional sensor beyond that would reduce this number to 101 (Case 5).

"combined" indicates that there is a combination of structural systems along the height of the building. So, out of the listed 102 buildings, we only analyzed specific direction(s) of buildings whose instrumentation layouts are labeled as "Y" and whose structural systems are not "combined". Also, we deselected very short buildings (most stiff buildings that are less than 5-story high), to make sure that there are at least two contributing modes, because the proposed identification method requires modal superposition. It is also useful to note here that various metadata errors were encountered in some of the buildings (e.g., CSMIP 58479, CSMIP 3300, CSMIP 24232, etc.), and these stations are therefore excluded them from the study, even though they nominally satisfied the criteria mentioned above.

The final set of selected buildings is tagged by a **green color** and the analysis direction is displayed in the last column of the Table A. Finally, as seen, 21 steel (28 if each direction is counted as a building) and 40 concrete (65) buildings are analyzed in the present study by using the CSMIP-CIT toolbox.

Results

In this section, comprehensive results of the application of the proposed method to data from the selected buildings (see previous section) are presented. As there are several earthquake data sets for some of these buildings, we analyzed a total of **373** earthquake data sets. While the primary purpose of this study is to extract frequency-dependent soil-foundation Impedance Functions (IFs) and Foundation Input Motion (FIMs), we also investigated fixed-base-system modal properties as a byproduct of this study. Therefore, in the following sub-sections, we present results on both the superstructure (i.e., fixed-based-system) and the overall (structure-foundation-soil) flexible-base system properties. The proposed identification method allows an accurate delineation of the superstructure flexible-base system properties, whether the building as a whole exhibited/experienced SSI effects (foundation sway/rocking) or not.

After the superstructure properties are discussed and comparisons of fixed- and flexible-based system properties are made, the results for flexible-base systems are presented in more detail. In that sub-section, we provide specific examples of the identified IFs and FIMs, as well as aggregate results—such as those that demonstrate the amplitude- and frequency-dependency of IFs. It is also important to note here that some of the studied buildings' dynamic characteristics have apparently changed significantly over time (possibly due to earthquake damage, retrofitting efforts, or through the addition of seismic mitigation devices). In the present study, we also investigated such buildings separately so that the aggregation of identification results could be made properly.

Detailed results of all 373 analysis cases are presented in Appendix B, and further details are available in (Taciroglu et al., 2016c).

Key Observations

Permanent Changes

First, we present buildings whose dynamic characteristics have permanently changed, because of possible damage experienced in a severe earthquake event or due to elements added as part of a retrofit. Figure 7 shows fundamental flexible-base natural frequency of the Van Nuys

Hotel (CSMIP 24386) obtained from 5 earthquakes. As seen, there are two significant variations in the natural frequency. First, the fundamental natural frequency significantly drops during the 1994 Northridge Earthquake, indicating damage. The building was then retrofitted in the EW direction by adding several concrete shear walls. These additional shear walls increased the lateral stiffness, and consequently the natural frequency in the EW direction by a factor of 4 which are clearly seen from identified frequencies from two recent earthquakes—namely, 2008 Chino Hills and 2014 Encino earthquakes. Therefore, this building in the EW-direction must be considered as three different buildings—a different building each, for the Landers/Big Bear, Northridge, and Chino Hills/Encino earthquakes.

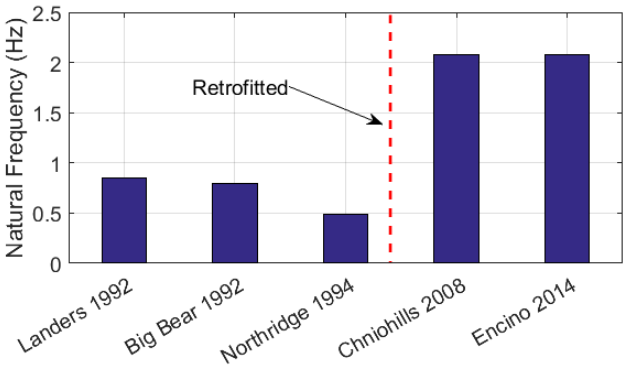

Figure 7. Chronological variation of flexible-base natural frequency of CSMIP 24386 in EW direction.

Figure 8 displays the fundamental flexible-base natural frequency of the CSMIP 24322 obtained from 5 earthquakes. This building has also experienced some damages during Northridge earthquake (1994), so it was retrofitted after this time. As it can be seen, natural frequency has significantly increased in three following earthquakes after 1994. Hence, this building in EW direction should be considered as two different buildings, one before 2008 and one after this year.

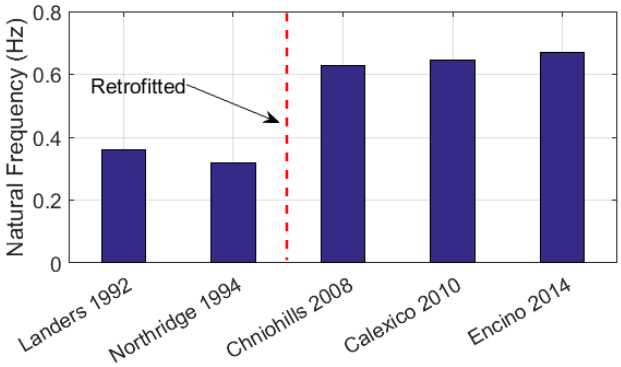

Figure 8. Chronological variation of flexible-base natural frequency of CSMIP 24322 in EW direction.

Note that these two buildings are stations whose retrofit (permanent change) are clearly stated in the CESMD. Otherwise, by looking at flexible-base natural frequency, it is not reliable to conclude about permanent structural variations, because both the soil and the structural nonlinearities can cause frequency reductions. For example, the variation of the flexible-base natural frequency of CSMIP 12299 in three earthquakes is shown in Figure 9. As seen, the

flexible-base natural frequency varies from earthquake to earthquake. However, the fixed-base natural frequency is almost constant. So, by comparing these two frequencies, we can conclude that this building's superstructure has not experienced any damage

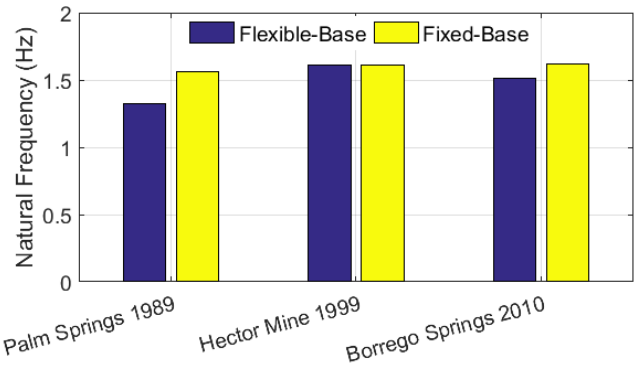

Figure 9. Chronological variation of fixed- and flexible-base natural frequencies of CSMIP 12299 in the EW-direction.

With this in mind, we can study the CSMIP 24386 and 24322 buildings again. Our analysis shows that CSMIP 24322 is fixed-base structure, but CSMIP 24386 has foundation sway. Figure 10 displays a similar graph as Figure 7 but this time fixed-base natural frequencies are used. This figure is in agreement with what we concluded from Figure 7. Also, by comparing this figure with Figure 7, we can conclude that level of soil and structural nonlinearity is different for the Landers and the Big Bear earthquakes.

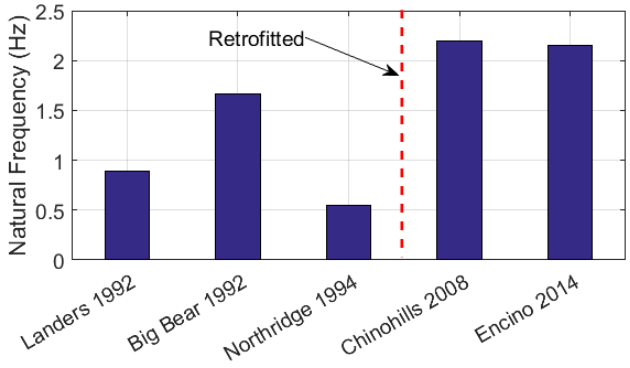

Figure 10. Chronological variation of the fixed-base natural frequency of CSMIP 24386 in the EW-direction.

To show the importance of the fact mentioned above, it is useful to look at the variation of the flexible-base natural frequency of CSMIP 57355 in the EW-direction during three earthquakes. As seen in Figure 11, the frequency goes down during the 1989 Loma Prieta earthquake in comparison to the 1984 Morgan Hill earthquake; and then it goes up again during the 2007 Alum Rock earthquake. Using only the *flexible-base natural frequencies*, it is possible to reach three different conclusions for the observed variation: (1) the building can be fixed and the observed variation is only due to the structural nonlinearity without permanent damage; (2) the building is a flexible-base structure and this variation is related to soil nonlinearities; and finally (3) the structure is damaged but the level of soil nonlinearity is masking this. Without the additional information provided by the fixed-base properties, it is not possible to distinguish

between the three possibilities. Fortunately, by having identified the fixed-base natural frequencies, we can offer a clearer interpretation of what has happened to this building.

As it can be seen in Figure 11, the fixed-base natural frequency does not change after its drop during Loma Prieta earthquake, so the building has likely suffered a permanent damage during that 1989 event. Due to the higher level of excitation during the Loma Prieta earthquake, soil has also experienced larger strains, and hence there is a difference between the flexible-base and fixed-base natural frequencies in this earthquake, while this pattern is not seen in the Alum Rock 2007 earthquake data. Therefore, this building in the EW-direction should be treated as *two different* buildings for data before and after the Loma Prieta earthquake (1989).

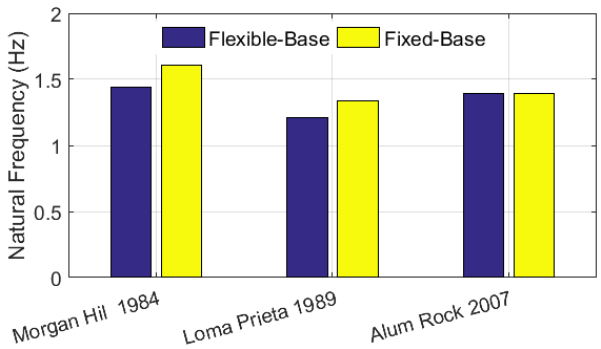

Figure 11. Chronological variation of fixed- and flexible-base natural frequencies of CSMIP 57355 in EW direction.

The last building in which we could identify permanent damage is the CSMIP station 12284 in the NS-direction. As seen in Figure 12, after the 1986 Palm Springs earthquake, there is a permanent stiffness reduction in this building. Note that the current approach to identify permanently changed buildings cannot be used for those buildings that have frequency drops only during their latest earthquake, because we use an equivalent linearization method. For example, the frequency variation of CSMIP 24601 in three successive earthquakes in both directions is shown in Figure 13. As it can be seen, there is a drop during the last earthquake, but it is not possible to conclude at the present time whether this is due to a permanent damage or it is an equivalent frequency identified for a nonlinear system. In the present study, we consider such buildings as *undamaged* buildings.

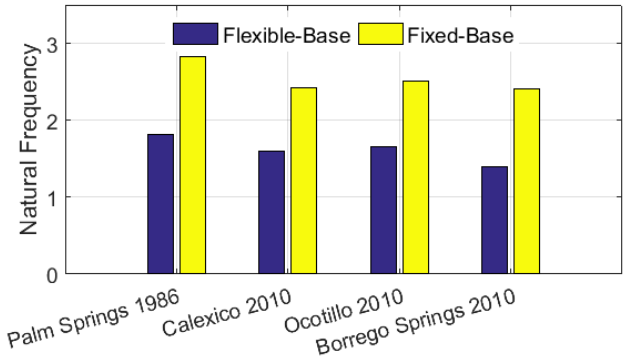

Figure 12. Chronological variation of fixed- and flexible-base natural frequencies of CSMIP 12284 in the NS-direction.

In addition to the permanent changes due to changes in stiffness, one of the buildings under study was equipped with dampers. Herein, we examine whether this building should be considered as a single case or not. Figure 14 shows variation of the damping ratio of the CSMIP 57357 in the EW-direction obtained from 5 earthquakes. This building has been equipped with dampers after the Loma Prieta earthquake. As expected, the building's damping ratio has increased after this earthquake, as it can be seen in Figure 14. To make sure that this damping increase is due to the additional dampers, and not the earthquake intensity (because it is well accepted that damping is significantly amplitude-dependent), we have added the variation of the Peak Foundation Acceleration (PFA) during these five earthquakes. As this figure shows, while level of excitation is much lower in the Milpitas (2010) and the Morgan Hill (2011) earthquakes, the level of identified damping ratios is still higher than previous earthquakes, which clearly indicates the contribution of the installed dampers. So, for interpretation of the identified damping, this building should be considered as two buildings, one before 1989 and one after this year.

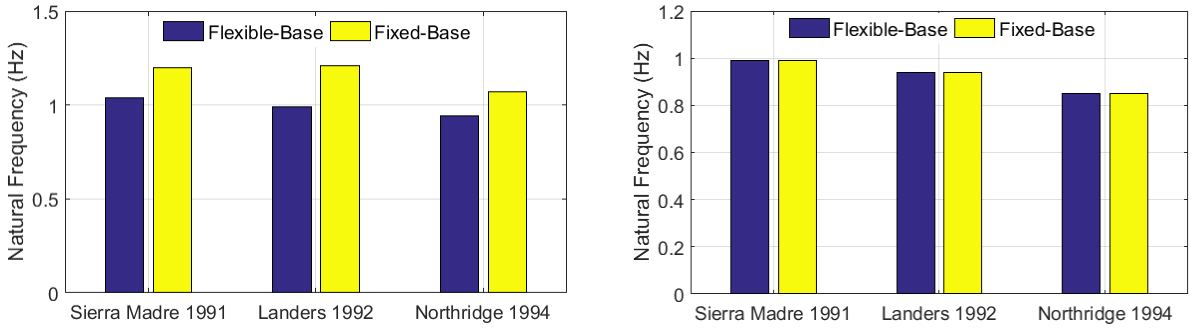

Figure 13. Chronological variation of fixed- and flexible-base natural frequencies of CSMIP 24601 in (left) EW and (right) NS-directions.

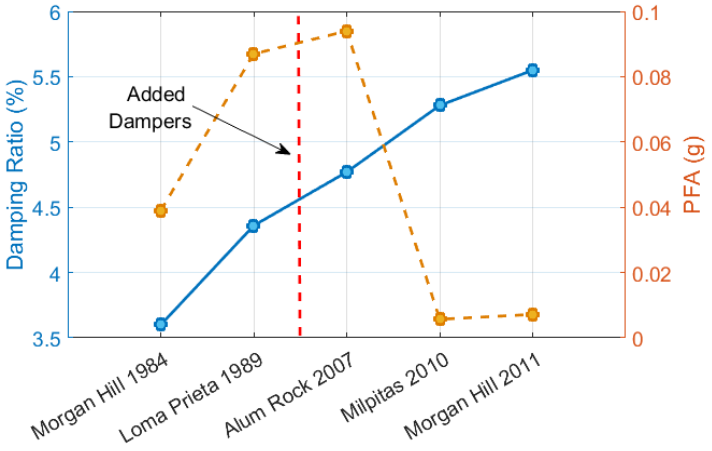

Figure 14. Chronological variation of flexible-base damping ratio and Peak Foundation Acceleration (PFA) of CSMIP57357 in EW direction.

In concluding this section, we now consider and implement the changes listed in Table 3 into our CSMIP-CIT database for future analyses.

Table 3. Modifications to the database due to permanent changes in buildings.

No.	CSMIP No.	Dir.	Case	Earthquakes
1	24386	EW	1	≤ 1992
			2	= 1994
			3	≥ 2008
2	24322	EW	1	< 2008
			2	≥ 2008
3	12284	NS	1	≤ 1986
			2	> 1986
4	57355	EW	1	≤ 1984
			2	> 1984
5	57357	NS, EW	1	≤ 1989
			2	> 1989

Soil and Structural Nonlinearities

In the previous section, we showed how to take advantage of the identified fixed- and flexible-base natural frequencies to identify and quantify the permanent changes in instrumented buildings, and to update the database accordingly. In this section, we investigate the observed nonlinear behavior in the soil-foundation system and/or the superstructure by using the identified fixed- and flexible-base natural frequencies. We need to carry out this investigation so that we can appropriately select data points in subsequent sections—e.g., to retrieve frequency-dependent soil-foundation impedance functions by aggregating results from several buildings. Before going through this investigation, it is worth noting that it is not appropriate to assign a single label—e.g., *fixed-base*—to a building. In other words, a building can behave in a fixed-based manner in an earthquake, and yet its foundation can move with respect to the ground during another event that has different level of intensity and/or frequency content. As an example, Figure 15 shows the frequency variation of CSMIP 58261 in the EW-direction during three different earthquakes. As seen, during the severe 1989 Loma Prieta earthquake (PFA = 0.16*g*, which is ~5 times higher than the two other earthquakes), there is significant soil-foundation flexibility. That is, this building behaved in a fixed-base manner in two earthquakes, but exhibited flexible-base response during the Loma Prieta earthquake.

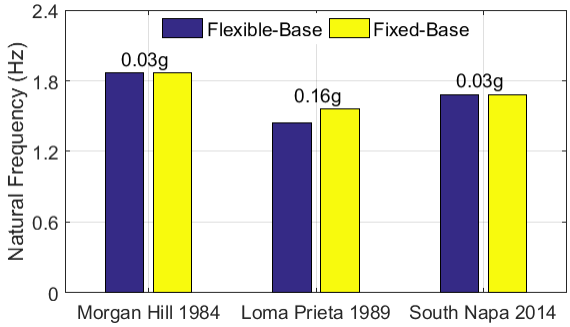

Figure 15. Chronological variation of fixed- and flexible-base natural frequencies of CSMIP 58261 in EW direction.

Excluding special cases like CSMIP 58261, we can generally classify buildings under study into following five groups according to the identified results[4]:

- *Linear Fixed-Base*: For these buildings, no sign of soil-structure interaction effect was observed in their analyzed earthquake data. Also, almost the same natural frequencies were obtained using different earthquakes. An example of such buildings is shown in Figure 16(a). As seen, a single type of natural frequency is shown, meaning that there was no soil-foundation flexibility. Also, the identified natural frequencies from 6 different earthquakes from 1978 to 2013 were almost equal.
- *Nonlinear Fixed-Base*: For these buildings, while the building is fixed at its base, the superstructure parameters significantly varied from event to event. As an illustration, the variation of natural frequencies of CSMIP 23511 (NS direction) is shown in Figure 16(b).
- *Linear Flexible-Base*: These types of buildings were flexible-base in all analyzed earthquake data sets (contrary to, for example, CSMIP 58261). However, there was less amplitude-dependency in both their fixed- and flexible-base properties. An example of such buildings is shown in Figure 17. As seen, the fixed- and flexible-base natural frequencies were constant from 2002 to 2014.
- *Flexible-Base with Nonlinear Soil-Foundation*: The difference between this group of buildings and the previous one is that while the superstructure has not changed in multiple earthquakes, the soil-foundation system exhibited amplitude-dependency. An example of these types of buildings is shown in Figure 18. As seen, while the fixed-base natural frequency is almost constant, the flexible-base natural frequency significantly varies from earthquake to earthquake.
- Nonlinear Flexible-Base: This group of building showed amplitude-dependency in both the substructure and the superstructure (we could not find cases for which the superstructure showed amplitude-dependency, while substructure did not). An example of these buildings is shown in Figure 19.

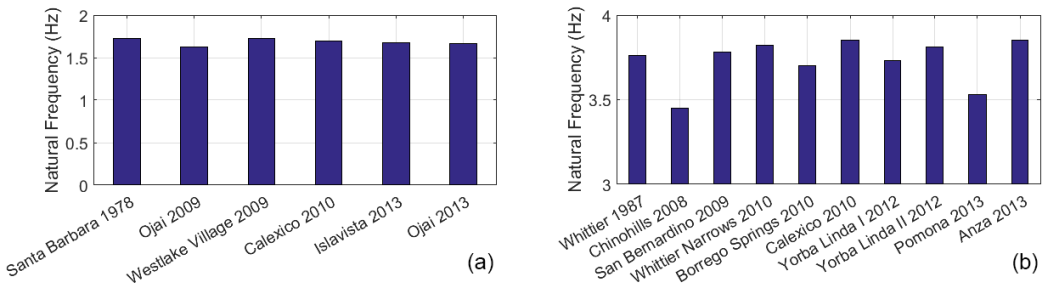

Figure 16. (a) CSMIP 25339-EW and (b) CSMIP 23511-NS representing linear and nonlinear fixed-base systems, respectively.

[4] It is obvious that this classification can change and become more refined by recording more earthquake data.

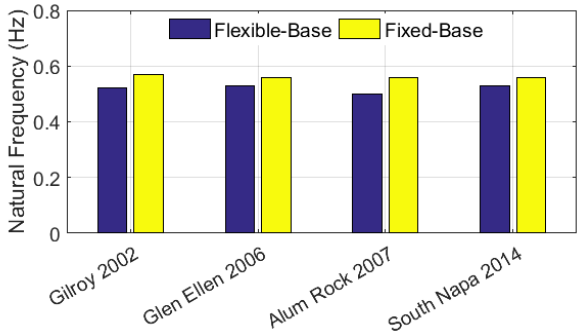

Figure 17. CSMIP 58615-EW as an example of linear flexible-base system.

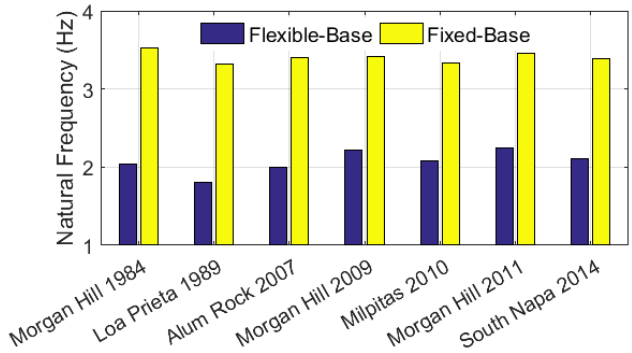

Figure 18. CSMIP 57356-EW as an example of nonlinear flexible-base system with linear superstructure.

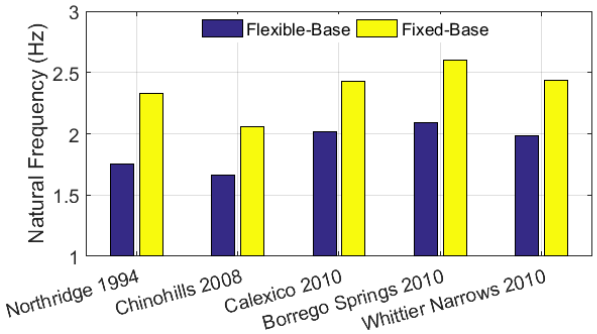

Figure 19. CSMIP 14606-NS as an example of nonlinear flexible-base system with nonlinear superstructure.

Superstructure Parameters

Natural Frequencies

Shear wave velocity in building structures can be used as a simple measure to predict their natural frequencies (in the fixed-base condition) (see, for example, Todorovska & Trifunac, 2008). Figure 20 shows the probability density function estimated from the identified shear wave velocity of the buildings using $\sqrt{G/\rho} = L/(\sqrt{k}s\bar{b})$. First, we neglect amplitude-dependency effects and use all available data points. As seen in Figure 20(left), buildings with moment frames—i.e., Moment Resisting Steel Frames (MRSFs) or Reinforced Concrete Frames (RCFs)—have the lowest shear-wave velocity. It is worth noting that the mean value does not appear to depend on the material type, and is almost the same for both MRSFs and RCFs. This figure shows that the shear wave velocity in steel structures increases from MRSF to S-Dual to

BSF. This order is expected, because buildings with Braced Steel Frames (BSFs) usually have higher stiffness. A similar order is not completely established for concrete buildings, which may be due to two main reasons: First, amplitude-dependency plays a higher role for them, and/or there are misclassifications in the metadata. The latter reason is unlikely, because metadata did not bear many ambiguities. However, we can explore the former effect by using data from weak earthquakes. As such, we repeated Figure 20(left) on the right-side by using the weakest earthquake data (causing the highest fixed-base natural frequency). As seen, the aforementioned problem is almost removed. Also, the two-peak pattern already observed in Figure 20(left) for RCF, BSF, and CSW are significantly reduced in Figure 20(right). Finally, it can be seen from both figures that buildings having dual systems are mostly affected by the stiffest sub-system. That is, S-Dual is closer to BSF than MRSF and C-Dual is closer to CSW than RCF.

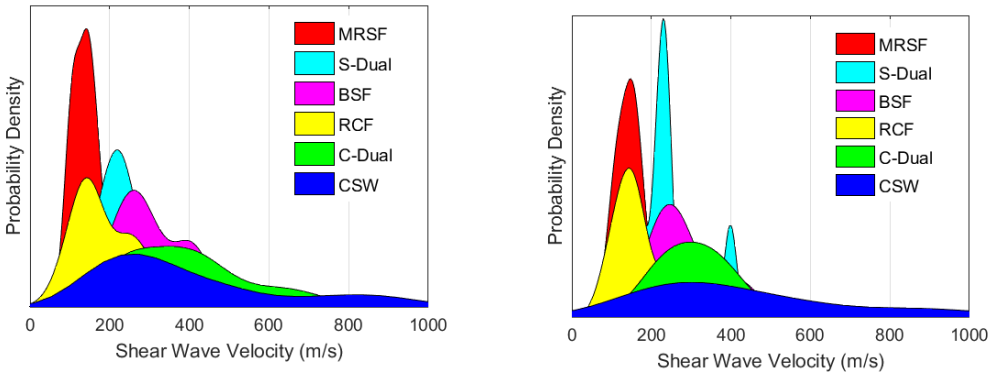

Figure 20. Probability distribution of shear wave velocity in fixed-base buildings. Left: full data, Right: weak earthquake data.

Having an average value of $\sqrt{G/\rho}$ for different types of structural systems as identified from Figure 20, we can predict the fixed-base natural frequency of any building through the Timoshenko beam model, if we can also have an estimation for shear-to-bending stiffness values—i.e., G/E. Using the identified parameters, we can back-calculate G/E as $I/(s^2 A_s L^2)$ for different types of structural systems. Histograms of G/E for all six structural systems are shown in Figure 21. Although the number of data points is limited in the current study, this approach can be used in the future when as a larger data set becomes available. G/E corresponding to the peaks of Figure 21 are reported in Table 4. Also, values of $\sqrt{G/\rho}$ corresponding to the peaks of Figure 20 are reported in this table. Now, it is possible to estimate fixed-base natural frequency of a building having a specific lateral system through the frequency equation of a fixed-base Timoshenko beam by using following parameters

$$\bar{b} = 3.46 \frac{1}{\sqrt{G/\rho}} \sqrt{G/E} \frac{L^2}{D} = \frac{3.46 L^2 \sqrt{\rho/E}}{D} \tag{13}$$

$$s = \frac{1}{3.19\sqrt{G/E}} \frac{D}{L} \tag{14}$$

Note that, a rectangular section has been assumed for deriving equation above.

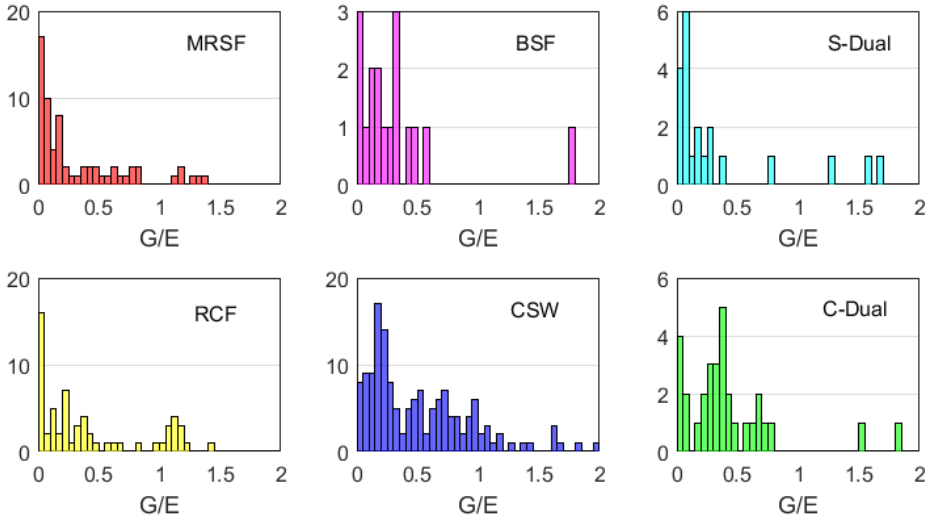

Figure 21. Histograms of identified G/E for various types of structural systems.

Table 4. Identified factors for natural frequency prediction.

Structural Type	G/E	$\sqrt{G/\rho}$ $(m/\sec^2)$
MRSF	0.03	148
BSF	0.03, 0.33	250
S-Dual	0.07	230
RCF	0.03, 0.23	144
CSW	0.17	300
C-Dual	0.37	300

Using Eqs. (13) and (14) and approximate values presented in Table 4, the fixed-base natural frequencies of buildings for a wide range of structural height and plan-depth are plotted in Figure 22. In this figure, we also show actual building data points (for BSF and RCF, we used G/E equal to 0.03 and 0.23, respectively). As it can be seen from this figure, the proposed values for Timoshenko beam model can represent the average behavior of all Timoshenko beam models identified for buildings under study.

Herein, we compare our predictive formulas for fixed-base natural frequencies with other available formulas. These reference formulas are summarized in Table 5 and their details and history can be found in (Taciroglu et al., 2016c). As seen on Table 5, there is no prior study in which the fixed-base natural frequency is explicitly extracted from real-life data. However, it should be made clear that if the buildings under investigation in any of the studies listed in Table 5 were physically fixed-base, then the identified flexible-base or pseudo-flexible base natural frequencies should be comparable with our results. Herein, we compare our results with those formulas available in the latest version of the ASCE-7, 2010. Figure 23 presents this comparison for four types of structural systems[5]. As seen, for tall buildings in which SSI is mostly negligible,

[5] We did not carry out a comparison for CSW and C-Dual systems, because the ASCE-7 formulae for these systems require detailed information on shear walls.

the formula presented in ASCE 7-10 is nearly matched to the fixed-base natural frequencies we predict for plan-depth of ~80 m, which is expected. However, for short structures for which SSI effects have a higher proportion of contribution to the overall response, the fixed-base natural frequencies identified here are larger than that from the ASCE formula. This suggests that there is an implicit portion of soil-foundation flexibility (pseudo-flexible base) embedded in the ASCE formula. Moreover, the observed difference is much larger for systems having BSFs, which are stiffer in comparison to three other systems.

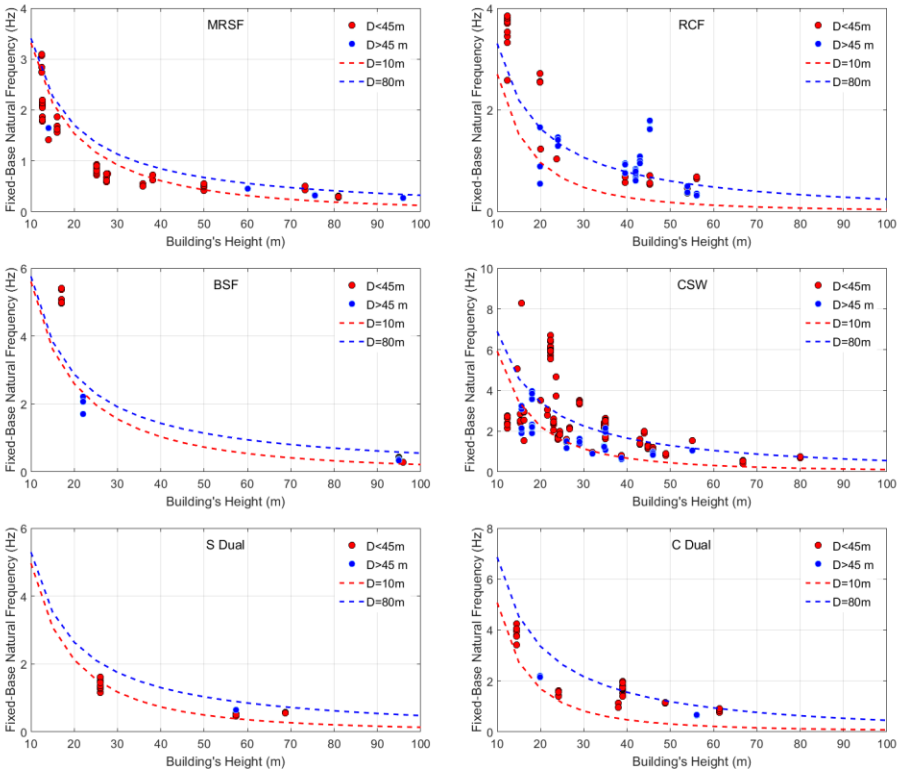

Figure 22. Fixed-base natural frequency predicted for various structural systems.

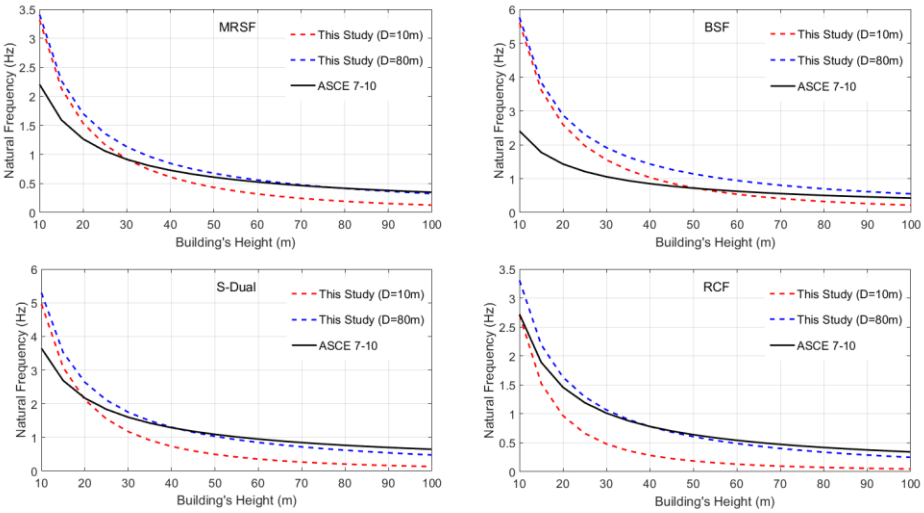

Figure 23. Comparison between fixed-base natural frequency predicted by the present study and ASCE 7-10 (2010) for various structural systems.

Table 5. Available approximate formulae for estimating the fundamental natural frequencies (in the expressions below, f_1 is in Hz, the building dimensions L and D are in feet. N denotes number of stories, and A_e is the effective area defined in Goel & Chopra, 1998).

Case	Proposed Formula	Building Type	Base* Condition	Developers	Reference
1	$f_1 = 33L^{-3/4}$	RCF	Pseudo-Flexible	UBC97, NEHRP94, SEAOC96	(UBC, 1997; NEHRP, 1994; SEAOC, 1996)
2	$f_1 = 40L^{-3/4}$	RCF	Pseudo-Flexible	ATC3-06	(ATC, 1978)
3	$f_1 = 29L^{-3/4}$	MRSF	Pseudo-Flexible	ATC3-06, UBC97, NEHRP94, SEAOC96	(ATC, 1978; UBC, 1997; NEHRP, 1994; SEAOC, 1996)
4	$f_1 = 50L^{-3/4}$	CSW	Pseudo-Flexible	NEHRP94, SEAOC96	(NEHRP, 1994; SEAOC, 1996)
6	$f_1 = 20D^{1/2}L^{-1}$	CSW	Pseudo-Flexible	ATC3-06	(ATC, 1978)
7	$f_1 = 11D^{1/2}L^{-1}$**	CSW	Pseudo-Flexible	NBCC95	(NRC, 1995)
8	$f_1 = 56L^{-1}$**	RCF	Flexible	Lagomarsino	(1993)
9	$f_1 = 59L^{-0.92}$	RCF	Pseudo-Flexible	Goel & Chopra	(1997)
10	$f_1 = 29L^{-0.805}$	MRSF	Pseudo-Flexible	Goel & Chopra	(1997)
11	$f_1 = 435L^{-1}A_e^{0.5}$	CSW	Pseudo-Flexible	Goel & Chopra	(1997)
12	$f_1 = 100L^{-1}$**	CSW	Flexible	Farsi & Bard	(2004)
13	$f_1 = 20L^{-3/4}$**	CSW	Pseudo-Flexible	NRC/IRC 2010	(NRC/IRC, 2010)
14	$f_1 = 58L^{-1.032}$**	CSW	Flexible	Gilles & McClure	(2012)
15	$f_1 = 36L^{-0.8}$	MRSF	Pseudo-Flexible	ASCE 7-10	(2010)
16	$f_1 = 50L^{-0.75}$	S-Dual	Pseudo-Flexible	ASCE 7-10	(2010)
17	$f_1 = 63L^{-0.9}$	RCF	Pseudo-Flexible	ASCE 7-10	(2010)
18	$f_1 = 33L^{-0.75}$	BSF	Pseudo-Flexible	ASCE 7-10	(2010)

* This is the actual base condition not the purpose of the usage. Indeed, natural frequencies estimated from approximate formulas of building codes are usually assumed fixed-base.

** Dimensions in this formula are in meters.

Damping Ratios

Building damping is one of the most challenging parameters to estimate in earthquake engineering, as it is not directly computable and many factors contribute to it. Due to this ambiguity, as well as computational convenience, viscous damping models are usually used, whereas the inherent damping responses of structural systems are not necessarily so. As modal combination has been the basis of all classic seismic design, damping had been specified by defining modal damping ratios. As these parameters cannot be directly derived from first principles at the present time, identification of damping ratios from real-life vibration data is the only viable path to quantification. While this route has been known, there have been only a few attempts to date to relate damping ratios to detailed specifications of structures, because of

ambiguities in damping sources, inadequacies of data, and the inabilities of identification methods, as well as inherent uncertainties in the identification processes (Kijewski-Correa & Pirnia, 2007). Not surprisingly, seismic design codes could only provide general and vague recommendations, and usually constant damping ratios for many years (%5 for concrete/masonry structures and %2 for steel structures). For example, in the latest version of ASCE 7-2010 (ASCE7-10, 2010), the word damping is mentioned many times in many sections, but without any specific values. Here are a few examples, which are originally collected by Miranda (2014):

- Section 16.1.2: "*Mathematical models shall conform to the requirements of Section 12.7*," yet there is nothing about damping specifications in Section 12.7.
- Section 17.6.3.3: "Response-spectrum analysis shall be performed using a modal damping value for the fundamental mode in the direction of interest not greater than the effective damping of the isolation system or 30 percent of critical, whichever is less. Modal damping values for higher modes shall be selected consistent with those that would be appropriate for response spectrum analysis of the structure above the isolation system assuming a fixed base," yet the appropriate damping ratio for a fixed-base structure is not known.
- In one of the rare cases, in Section 12.9 (Modal Response Spectrum Analysis), the recommendation is to use the 5% damped spectrum as input that is using 5% damping ratios for all structures and modes.

A number of researchers suggested simplified formulae for first mode damping ratios using different parameters and calibrated these by using damping ratios estimated/identified from vibration data. Building height, material type, and vibration intensity were utilized as the primary physical parameters on these approximations. A short list of these studies is shown in Table 6 and further details can be found in (Taciroglu et al., 2016c).

Table 6. Presently available approximate formulas for building damping ratios.

Case	Proposed Formula	Building Type	Base Condition*	Developer(s)
1	$\xi_1 = \frac{0.3192}{f_1} + 0.7813 f_1$	Steel	Unknown	(Lagomarsino, 1993)
2	$\xi_1 = \frac{0.7238}{f_1} + 0.7026 f_1$	Concrete	Unknown	(Lagomarsino, 1993)
3	$\xi_1 = \frac{0.2884}{f_1} + 1.2856 f_1$	Mixed	Unknown	(Lagomarsino, 1993)
4	$\xi_1 = 1.945 + 0.195 {f_1}^{3.779}$	Mixed	Flexible	(Zhang & Cho, 2009)
5	$\xi_1 = 8.07 L^{-0.25}$**	Steel	Mixed	(Fritz et al., 2009)
6	$\xi_1 = 25.36 L^{-0.5}$**	Concrete	Mixed	(Fritz et al., 2009)
7	$\xi_1 = 1\ (L < 100)$, $\xi_1 = 198 L^{-1} (L > 100)$ **	Steel	Flexible	(PEER/ATC, 2010)
8	$\xi_1 = 2 (L < 100)$, $\xi_1 = 330 L^{-1} (L > 100)$ **	Concrete	Flexible	(PEER/ATC, 2010)
9	$\xi_1 = 1.2 + 4.26 e^{-0.013L}$**	Steel	Pseudo-Flexible	(Bernal et al., 2013, 2015)
10	$\xi_1 = 3.01 + 3.45 e^{-0.019L}$**	Concrete	Pseudo-Flexible	(Bernal et al., 2013, 2015)

* This is the actual base condition not the purpose of the usage. Indeed, natural frequencies estimated from approximate formulas of building codes are usually assumed fixed-base.
** Building height is in meters.

The results of the present study are universal in that the damping ratios identified here are only due to superstructure behavior (but not polluted by SSI effects, which should be considered and treated separately). Figure 24 shows the identified fixed-base damping ratio versus natural frequency for four structural types. Unfortunately, for CSW and C-Dual systems, we could not determine any pattern for the damping ratio. One reason for this is probably due to the amplitude-dependency, which can significantly alter damping levels in buildings having shear walls. For all other systems, we could extract a relationship between the fundamental natural frequency and the damping ratio. We selected natural frequency as the regression metric, because it produced much better fitness values in comparison to, for example, building height. Considering friction within connections or among elements, as well as the density of the presence of non-structural elements, we expect to see a direct correlation between the fixed-base natural frequency and fixed-base damping ratio. This expectation is confirmed and evident in Figure 24. Analytical formulae corresponding to the fitted curves of Figure 24 are presented in Table 7. With these expressions, it is now possible to first calculate the fixed-base natural frequencies using formulae proposed in the previous section, and then to predict the fixed-base damping ratio for the superstructure. Having the superstructure damping and the foundation damping, which will be the discussed in the next section, any SSI system can be analyzed using the substructure approach.

Table 7. Proposed approximate fixed-base damping ratios.

Case	System	Equation	R^2
1	MRSF	$\xi_1 = -5.83{f_1}^{-0.30} + 12.76$	0.33
2	RCF	$\xi_1 = 3.06{f_1}^{-1.01} + 2.23{f_1}^{-0.85}$	0.19
3	S-Dual	$\xi_1 = 2.44f_1 + 2.51$	0.19
4	C-Dual	---	---
5	BSF	$\xi_1 = 1.16f_1 + 3.44$	0.41
6	CSW	---	---

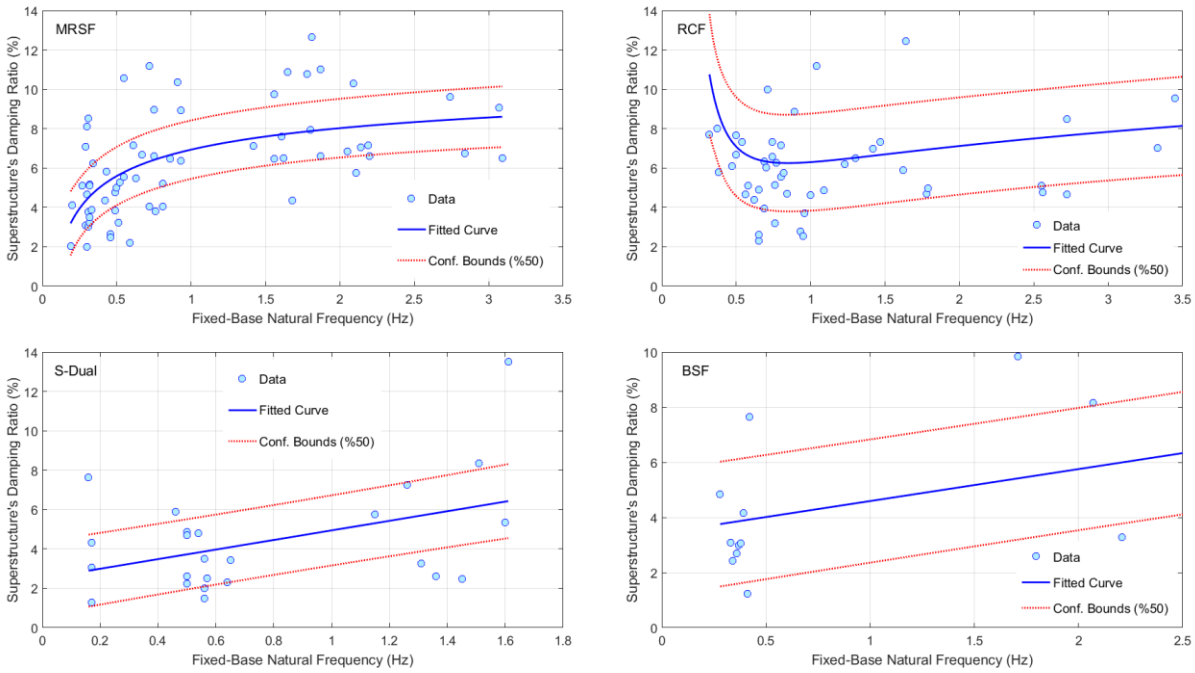

Figure 24. Variation of superstructure first mode's damping ratio versus fundamental fixed-base natural frequency and fitted curves along with their %50 confidential bounds.

Soil-Foundation Parameters

Frequency-Dependency

According to ASCE 7-10 (2010), requirements of Chapter 19 are permitted to be used in the determination of the earthquake-induced forces, if the building is flexible-base and the superstructure is modeled as fixed-base. Based on these requirements, there are two SSI-related parameters that control the base shear reduction subject (cf. Eq. 19.2-1 of ASCE 7-10). These two parameters are flexible-base natural period (T_{Flex}) and soil-foundation-structure damping ratio (ξ_{Flex}). T_{Flex} is determined based on the formulation derived by Veletsos and Meek (1974) using a SDOF structure placed on a sway-rocking foundation, and is given by

$$T_{Flex} = T_{Fixed}\sqrt{1 + \frac{\bar{k}}{K_T}\left(1 + \frac{K_T h^2}{K_R}\right)} \qquad 15)$$

where $\bar{k} = 4\pi^2 \bar{W}/\left(g{T_{Fixed}}^2\right)$ is the stiffness of the superstructure; T_{Fixed} is the fixed-base natural period; h and $\bar{W}$ are the effective height and weight of the superstructure at its first mode (typically assumed as %70 of the building's height and weight); and K_T and K_R are the soil-foundation sway and rocking stiffnesses, respectively. To calculate the soil-foundation stiffnesses, "*established principles of foundation mechanics using soil properties that are compatible with the soil strain levels associated with the design earthquake motion*" are to be used. Alternatively, "*for structures supported on mat foundations that rest at or near the ground surface or are embedded in such a way that the side wall contact with the soil is not considered to remain effective during the design ground motion, the effective period of the structure is permitted to be determined from*:

$$T_{Flex} = T_{Fixed}\sqrt{1 + \frac{25\alpha r_T h}{{V_s}^2 {T_{Fixed}}^2}(1 + \frac{1.12 r_T h^2}{\alpha_R {r_R}^3})}. \quad 16)$$

The equation above can be rewritten as

$$T_{Flex} = T_{Fixed}\sqrt{1 + \frac{\bar{k}}{K_T^{ST}}(1 + \frac{K_T^{ST} h^2}{\alpha_R K_R^{ST}})} \quad 17)$$

where K_T^{ST} and K_R^{ST} are the static sway and rocking soil-foundation stiffnesses for an equivalent circular foundation, which are calculated as

$$K_T^{ST} = \frac{8\,\rho {V_s}^2 r_T}{2 - \nu} \quad 18)$$

$$K_R^{ST} = \frac{8\,\rho {V_s}^2 {r_R}^3}{3(1 - \nu)} \quad 19)$$

where ν is the soil's Poisson ratio, and has been assumed 0.4 in Eq. (22). The parameters r_T and r_R denote the radius of the circular foundation that has an equal area and moment of inertia with the actual foundation, respectively. Eq. (17) indicates that the sway soil-foundation stiffness is assumed to be frequency-independent in ASCE 7-10, whereas a frequency-dependent factor α_R is considered for the rocking DOF. The value of this modification factor is obtained from Table 19.2-2 of ASCE 7-10 using the dimensionless parameter $r_R/(V_s T_{Fixed})$, which represents the superstructure-to-soil stiffness ratio.

Using our identified mass-normalized sway and rocking stiffnesses, we can evaluate how accurate the ASCE 7-10 recommendations—i.e., frequency-independent sway stiffness and α_R of Table 19.2-2—are. To carry out the said evaluation, we select data points that exhibited SSI effects (having different fixed- and flexible-base natural frequencies). Then, we multiply the mass-normalized stiffnesses of all buildings with $400L \times B \times D$ as an estimation of the total mass of the building. Next, we scale the recovered stiffnesses by static stiffnesses calculated by Eqs. (18) and (19) for sway and rocking, respectively. To use those formulas, we use small-strain shear wave velocity of site soils reported at the nearest CSMIP ground motion station (CESMD). To eliminate (or at least reduce) amplitude-dependency, we scale these shear wave velocities based on the recorded Peak Foundation Accelerations as recommended in (Givens, 2013).

Results of the identified rocking modification factors, α_R, versus the corresponding $r_R/(V_s T_{Fixed})$ are shown in Figure 25(a) as circle marks. For comparison purposes, the values recommended by ASCE 7-10 are also shown with continuous piecewise linear curves. As the maximum value of $r_R/(V_s T_{Fixed})$ in ASCE 7-10 is 0.5, we extrapolated the curve per the linear reduction of α_R after $r_R/(V_s T_{Fixed}) = 0.5$. As it can be seen, while a decreasing pattern is observed in the identified data, there is a large variability. However, the results this figure should be carefully interpreted, because we adopted several simplified assumptions (following ASCE 7-10) to carry out the comparisons. For example, we assumed that all buildings have a mass calculated using $400L \times B \times D$, all soil shear wave velocities are accurate and are correctly

scaled versus Peak Foundation Acceleration (PFA), the entire foundation contributes to the soil-foundation stiffness, and the formula used for static stiffness is accurate. Of course, it is not reasonable to expect that all of the said assumptions are valid for all of the buildings. As such, dividing the identified data into subcategories may provide a better understanding of the shortcomings of the ASCE provisions. For this purpose, we replot Figure 25(a) by clustering the results from different buildings into groups based on their common specifications in Figures 25(b-d). For example, Figure 25(b) displays data for different structural systems in a color code. As it can be deduced from these figures, most of the buildings whose identified frequency-dependent modification factor significantly deviates from the ASCE recommended values belong to non-CSW groups. This is likely because superstructures with CSW (Concrete Shear Wall) systems behave more like monolithic systems, which then allows the simplified modeling approaches that underlie the ASCE provisions to better approximate real-life behavior. This assertion is supported again by interpreting Figure 25(c), which delineates buildings with rigid (mat or interconnected) foundations whose lateral systems are not located as an interior core from those with flexible foundation systems. If we look at CSW systems with rigid foundations (Figure25d), then we find the greatest agreement between real-life data and ASCE 7-10 provisions. These results indicate that the frequency-dependent modification factors recommended in ASCE 7-10 are representative of a relatively narrow class superstructure-foundation systems, and may require amendments.

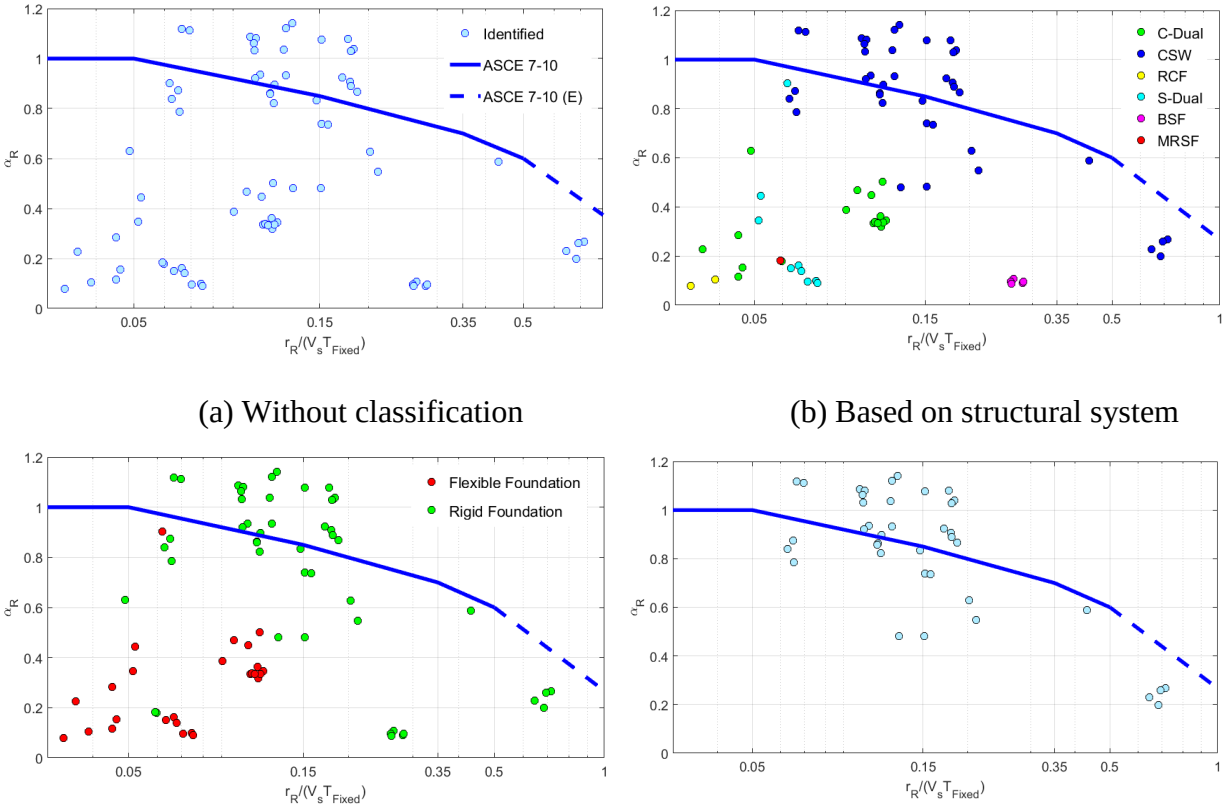

(a) Without classification

(b) Based on structural system

(c) Based on foundation rigidity

(d) CSW structures with rigid foundation

Figure 25. Comparison between identified and ASCE recommended α_R.

Frequency-dependent modification factors recommended by ASCE 7-10 are selected using the fixed-base natural periods, which is suitable for design procedures. However, as noted earlier, the primary objective of the present effort was to extract frequency-dependent soil-foundation impedance functions, which must be presented versus excitation frequency (here flexible-base natural frequency). To extract this information, we keep the vertical axes from Figure 25, but present results (for buildings with integrated foundations and CSW structural systems) versus dimensionless parameter $a_0 = \omega r/V_s$, wherein ω denotes the flexible-base fundamental frequency of each building. Figure 26 displays this graph along with the theoretical curve obtained by Veletsos and Verbic (1973), which is the basis for some of the ASCE 7-10 provisions on SSI, for comparison. As seen, the venerable Veletsos-Verbic approximation is in fair agreement with the field observations; nevertheless, the variability in the real-life data appears quite large and cannot be explained or captured by their model alone.

As mentioned above, and unlike the rocking stiffness, ASCE 7-10 (2010) provisions are based on the assumption that the foundation sway stiffness is not frequency-dependent. Figure 27 displays the α_R factor (i.e., frequency-dependency factor) for sway DOF values identified from CSMIP data versus the constant (unit) value recommended by ASCE 7-10. As seen, there is significant variability in real-life data, and this variability is most likely due to amplitude-dependent behavior of sway stiffness as well as uncertainties associated with field shear wave velocity data. Similar to Figure 26, the frequency-dependency of the sway stiffness is compared the analytical formula by Veletsos and Verbic (1973) in Figure 34. As seen, a frequency-independent factor appears to be a very good assumption for the sway stiffness.

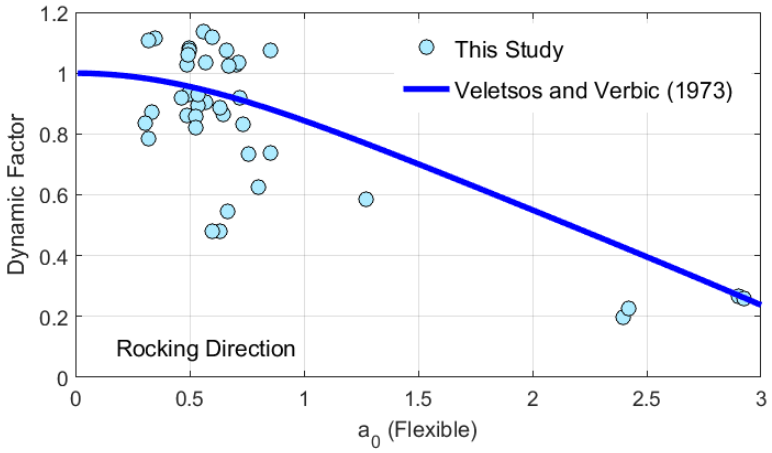

Figure 26. Frequency-dependency of soil-foundation rocking stiffness from CSMIP strong motion data versus the analytical solution by Veletsos and Verbic (1973) .

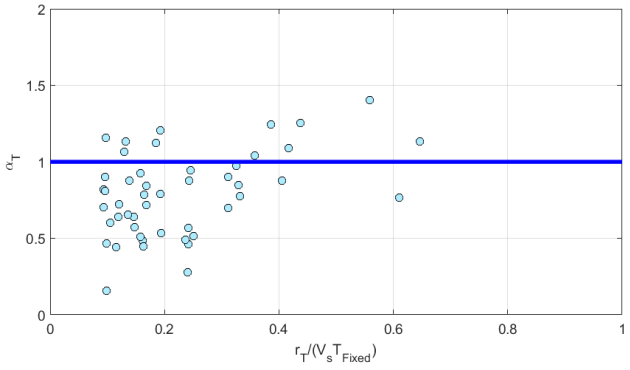

Figure 27. Frequency-dependency of the soil-foundation sway stiffness versus the ASCE 7-10 recommendation.

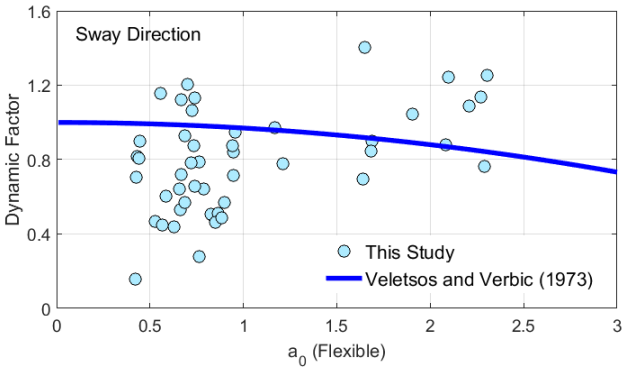

Figure 28. Frequency-dependence of soil-foundation sway stiffness versus Veletsos and Verbic (1973).

The effective damping ratio for the soil-foundation-structure system, ξ_{Flex}, is another parameter required for SSI analyses, and ASCE 7-10 recommends following formula to estimate it

$$\xi_{Flex} = \xi_0 + \frac{0.05}{\left(\frac{T_{Flexible}}{T_{Fixed}}\right)^3} \qquad 20)$$

where ξ_0 is damping associated with the soil-foundation system, which includes both hysteretic and radiation damping. This formula is based on the earlier studies, including that by Veletsos and Nair (1975) who showed that the damping ratio of the soil-structure system can be calculated through the following formula using fixed-base damping ratio ξ_{Fixed}

$$\xi_{Flex} = \xi_0 + \frac{\xi_{Fixed}}{\left(\frac{T_{Flexible}}{T_{Fixed}}\right)^n} \qquad 21)$$

where the exponent n depends on the type of damping (3 for viscous and 2 for hysteretic). By comparing Eq. (21) and (20), it is clear that an exponent of n = 3 and a superstructure damping of %5 are assumed in ASCE 7-10. To calculate the foundation damping ξ_0, a curve is provided in ASCE 7-10 based on the work by Veletsos and Verbic (1973), which relates the foundation damping to period elongation ($T_{Flexible}/T_{Fixed}$). However, it was later determined that the said curve was incorrectly produced by using the a_0 (introduced earlier) at fixed-base frequency instead of the flexible-base frequency (Givens, 2013). Therefore, herein, we calculate ξ_0 using Eq. (21) with n = 3 and the identified ξ_{Flex}, ξ_{Fxed}, T_{Fixed}, and $T_{Flexible}$ values, and compare our results with those predicted by Veletsos and Nair (1975), which supersedes the approach in (Veletsos & Verbic, 1973). Figure 29 presents the said comparison. This figure shows the identified and predicted foundation damping values versus $h/(V_s T_{Fixed})$. It is well accepted that the slenderness ratio of the building, h/r, plays an important role in foundation damping, and as such we present results for two levels of h/r (it is worth noting here that almost all our data

points have slenderness ratios below 2). Theoretically, the foundation damping decreases with increasing h/r, and this trend is also reflected in the identified damping values. However, results in Figure 29 also indicate that the code-based estimates (here, Veletsos & Nair, 1975) of foundation damping are generally higher then real life data.

Amplitude-Dependency

In the previous sections, we attempted to avoid the inherent amplitude-dependency of superstructure and soil-foundation impedance functions by using only low-intensity earthquake data, and by *correcting* the soil shear wave velocities, respectively. In this section, through a single case study, we show that soil nonlinearity is ever-present and must be well studied. We also show that while soil-nonlinearity is a challenge for our purposes in the present study, data recorded by instrumented buildings can be used to even identify nonlinear soil behavior—a task which is nominally carried out only through laboratory experiments (or sometimes using geotechnical downhole array data).

To demonstrate how the soil nonlinearity can alter the modal characteristics of a flexible-base system, the time-history and time-frequency distribution of the roof acceleration of CSMIP station #57356 recorded during 8 earthquakes (ranging from the 1984 Morgan Hill to the 2014 South Napa events) are shown in Figure 30, as an example. As this figure indicates, there are significant temporal variations not only from earthquake to earthquake, but also during each event.

We carried out identification for CSMIP 57356 using several earthquake data sets. For the Loma Prieta earthquake, which was a severe event at this station, we carried out identification in four successive time segments. The idenitified rocking stiffnesses (mass normalized values) versus Peak Foundation Accelerations (PFAs) are shown in Figure 31. As seen, there is a clear amplitude-dependency. That is, the rocking stiffness decreases when the level of vibration increases. This figure also shows that the soil stiffness does not quickly recover. In other words, the identified rocking stiffnesses at the third and the final time-windows for the Loma Prieta earthquake (1989) are lower than those expected for the given earthquake intensity (MH84 and ML86 have nearly the same earthquake intensity as LP89-3 and LP89-4, respectively).

Here, we show that the observed amplitude-dependency is compatible with what we expect, and incidentally identify a new research avenue in which data collected by instrumented buildings can be used to study nonlinearity their supporting soil domain. For this purpose, we first have to translate the peak foundation (~ground) acceleration to shear strain. To do so, we use the following relationship between the maximum shear strain and amplitude of a vertically propagating sinusoidal shear wave (Beresnev & Wen, 1996),

$$|\gamma_{max}| = \frac{A}{2\pi f V_s} \qquad 22)$$

where A is the acceleration amplitude, f is the wave frequency, and V_s is the soil shear wave velocity. We use amplitude of the Fourier Transform of the foundation response at first mode's flexible-base natural frequency (f) as an approximation of A. For the shear wave velocity, we use the small strain value. Figure 32 presents the same data points of Figure 31 but in different

axes. The horizontal axis is now a shear strain, which is calculated through Eq. (22), and the vertical axes is the rocking stiffness scaled by the maximum value obtained among all data points during the 2009 Morgan Hill Earthquake. For comparison, we have shown the shear reduction curve suggested by Ishibashi and Zhang (1993). The best-fit curve is obtained when the plasticity index is adjusted to 0 (i.e., sandy soil). As seen, there is very good agreement between the theoretical formula and the identified values.

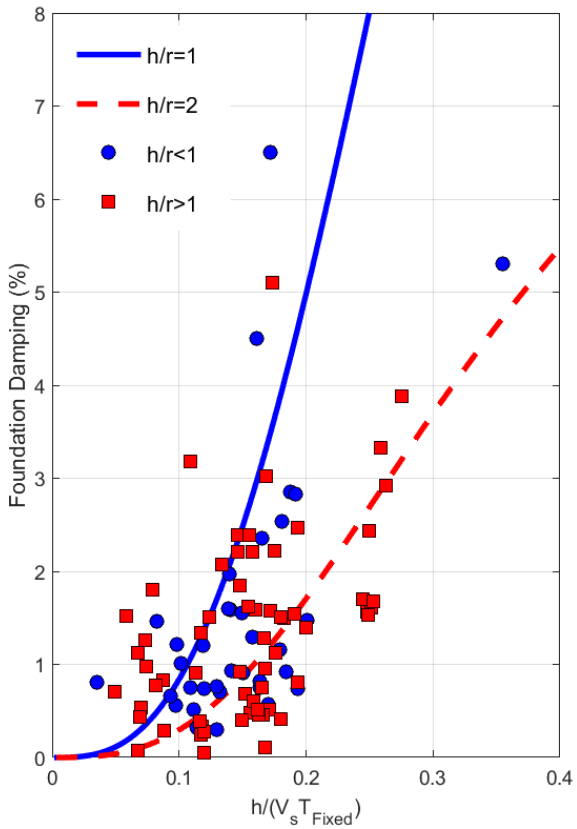

Figure 29. Comparison between identified (symbols) foundation damping values with those predicted using the model by Veletsos and Nair (1975) (solid lines).

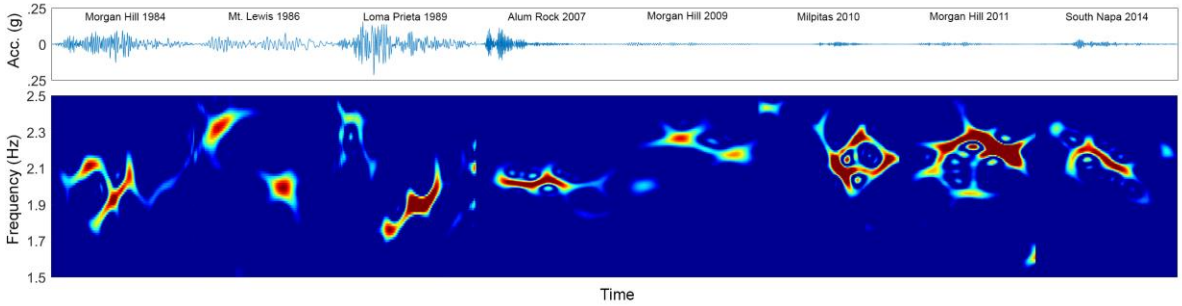

Figure 30. Time variation of the first natural frequency of CSMIP57356 during 8 earthquakes from 1984 to 2014[6].

[6] Colors do not reflect the actual signal energy at each time instant, because the signal has been scaled with its instantaneous amplitude to show its instantaneous frequencies more clearly.

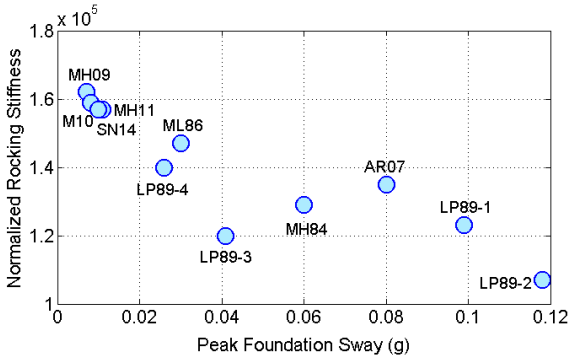

Figure 31. Amplitude-dependency of rocking stiffness observed at station CSMIP57356.

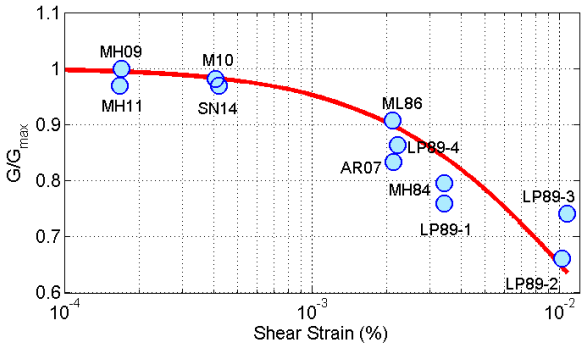

Figure 32. Soil shear modulus reduction identified in station CSMIP57356.

Kinematic Interaction/Foundation Input Motion

Kinematic Interaction (KI) is a relatively new consideration in seismic design/assessment codes (see, FEMA-440), because it is generally believed that total KI is somehow beneficial for the structure (Lin & Miranda, 2008). Moreover, the investigation of KI effects (except perhaps via analytical/numerical methods) is a challenging task because the Foundation Input Motions (FIMs) are not physically recordable. The present study is among the few efforts that offer a glimpse of FIMs extracted from real-life data, and opens a viable path towards the validation of numerical/analytical models of KI effects. An earlier study by Kim and Stewart (2003) has been one of the rare studies in this area. In that study, Kim and Stewart extracted the Transfer Functions between the nearby FFM and the recorded foundation motions. While such Transfer Functions embody KI effects, they do not isolate them, because the foundation motion is not generally equal to FIM (e.g., when foundation has a relative sway).

In the present study, we only tackle the horizontal FIM and neglect the rocking component, which is arguably a lesser effect for most structure-foundation systems (see, also, FEMA-400). It should be noted here, however, that the structure-foundation system is still allowed to rock, yet this rocking is only due to *inertial* rather than kinematic effects—which, for example, could be caused by surface or inclined body waves interacting with a large foundation slab (Mahsuli & Ghannad, 2009).

Figure 33 displays some of the identified FIMs for various buildings and earthquakes. As a rough comparison, the recorded foundation responses are also shown for each case. Note that the difference between these two signals is generated not by KI, but by inertial interaction. For cases that have an available nearby Free-Field Motion (FFM), we can now extract a Transfer Function between the recorded FFM and the recovered FIM, and subsequently compare this KI Transfer Function with those obtained through analytical/numerical models. As an example, Figure 34 displays the Transfer Function calculated between the FIM recovered for the 2011 Berkeley Earthquake from the transverse direction of Station 58503, and its nearby FFM station 58505. Per the recommendation by Kim and Stewart (2003), the Transfer Function is shown only for frequencies at which coherence (Pandit, 1991) is greater than 0.8. The theoretical Transfer Function for a rigid rectangular foundation with the same dimensions and shear wave velocity under vertical incoherent SH waves with incoherency factor of $\gamma = 0.5$ is also shown (Veletsos

et al., 1997). As seen, while the extracted Transfer Function is oscillatory, its mean value is in fair agreement with the theoretical prediction.

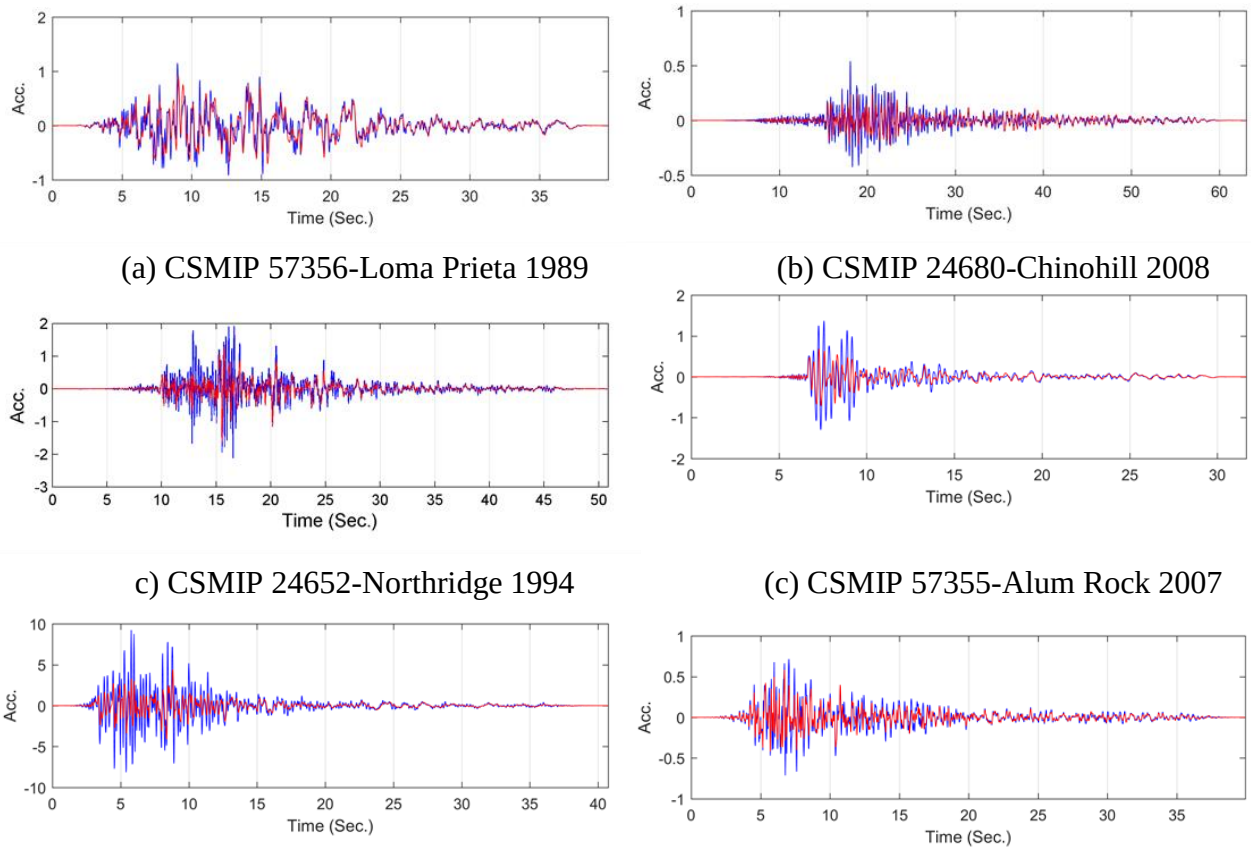

(a) CSMIP 57356-Loma Prieta 1989

(b) CSMIP 24680-Chinohill 2008

c) CSMIP 24652-Northridge 1994

(c) CSMIP 57355-Alum Rock 2007

(e) CSMIP 24386-Northridge 1994

(f) CSMIP 24332-Whittier 1987

Figure 33. Comparison between recorded the foundation responses and identified FIMs.

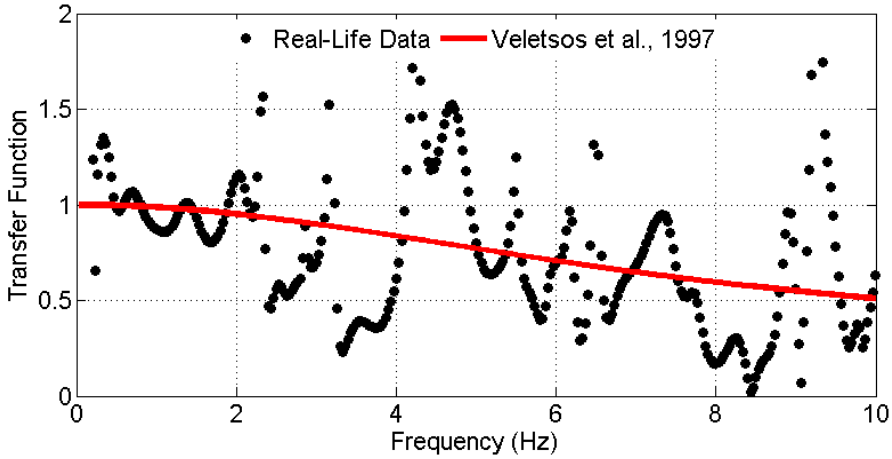

Figure 34. Comparison between the identified kinematic transfer function with that predicted through the model by Veletsos *et al.* (1997) using vertical incoherent shear wave formulation.

Conclusions

We presented the major findings of a two-year study on the identification of soil-foundation Impedance Functions and Foundation Input Motions from response signals of buildings instrumented through California Strong Motion Instrumentation Program (CSMIP). Based on station metadata and availability of records, we selected 373 earthquake data sets belonging to 61 building stations. Due to the nature of the identification problem at-hand, which required an output-only method suitable for non-stationary (i.e., strong earthquake) excitations, we devised a new method wherein the superstructure was modeled as a parametric (Timoshenko) beam for computational efficiency.

Major findings/outcomes of the obtained from the present study are:

- In order to carry out the voluminous data extraction, metadata classification, identification tasks, we developed a Matlab-based Toolbox called CSMIP-CIT. This toolbox is also able to automatically generate a concise report at the end of the analysis, and can be used in future research activities beyond the present effort.
- We developed approximation formulae to predict the fixed-base natural frequency of buildings using their plan dimensions and height, and the type of their lateral force resisting systems.
- We developed approximation formulae to predict the fixed-base damping ratios using fixed-base natural frequency.
- Identified results showed that, for buildings with Concrete Shear Wall (CSW) systems and integrated foundations, the presently available frequency-dependent soil-foundation stiffness modification factors in ASCE 7-10 are acceptable. For other building types and foundation systems, amendments may be appropriate.
- The current method for flexible-base damping ratio estimation of a soil-structure systems in ASCE 7-10 is based on a combination of fixed-base damping ratio (which is assumed to be 5%) and foundation damping, with combination weight calculated using the ratio of flexible-to-fixed base natural frequencies. However, we showed that the predicted foundation damping is generally non-conservative (i.e., higher than actual), especially for squat structures.
- The present study enabled the extraction of FIMs, and this can facilitate validation of numerical analyses (especially, those making use of direct finite element models) of Kinematic Interaction.
- While it was possible to extract FIMs for many CSMIP stations, lack of nearby Free-Field Motion stations prevents the extraction of direct KI Transfer Functions. For a single case whose FFM was available, we showed that a classic formula worked relatively well.
- The methods devised in the present study were also used the extract the amplitude-dependent (i.e., nonlinear) soil behavior; and the soil modulus reduction curve extracted from CSMIP data agreed with a theoretical formula quite well. This opens, again, the possibility to use field measured data from building structures to validate nonlinear

models of soil behavior—in effect, allowing the utilization of instrumented buildings as sensors to examine the behavior of the soils that support them.

Acknowledgments

The work presented in this manuscript was funded, in part, by the California Geological Survey (Contract No. 1014-963) and by the California Department of Transportation (Grant No. 65A0450). Authors are grateful for the support and assistance provided by Moh Huang and Anthony Shakal of California Geological Survey. Any opinions, findings, conclusions or recommendations expressed in this material are those of the authors and do not necessarily reflect the views of the sponsoring agencies.

References

Abrahamson, N.A., Schneider, J.F. & Stepp, J.C. 1991. Empirical spatial coherency functions for applications to soil-structure interaction analyses." *Earthquake Spectra,* 7(1), 1-27.

Aristizabal-Ochoa, J., 2004. Timoshenko beam-column with generalized end conditions and nonclassical modes of vibration of shear beams. *Journal of Eng. Mech.,* 130(10), 1151-1159.

ASCE (American Society of Civil Engineers), ASCE, 2010. *ASCE7-10: Minimum Design Loads for Buildings and Other Structures*, Report ASCE/SEI 7-10, Reston, VA.

ATC, (1978). Tentative provisions for the development of seismic regulations for buildings. Palo Alto, CA: Applied Technological Council.

Beresnev, I.A., & Wen, K. L., 1996. Nonlinear soil response—a reality?. *Bulletin of the Seismological Society of America*, 86(6), 1964-1978.

Bernal, D., Döhler, M., Kojidi, S. M., Kwan, K., & Liu, Y. 2015. First mode damping ratios for buildings. *Earthquake Spectra*, 31(1), 367-381.

Bernal, D., Kojidi, S.M., Kwan, K., & Döhler, M., 2013. Damping Identification in Buildings from Earthquake Records. In SMIP12 Seminar Proceedings, 39-56.

Bradford, S., Clinton, J., Favela, T. & Heaton, T., 2004. *Results of Millikan library forced vibration testing*: Earthquake Engineering Research Laboratory.

Çelebi, M., Firat, S. & Çankaya, I., 2006. The evaluation of impedance functions in the analysis of foundations vibrations using boundary element method. *Applied Mathematics and Computation*, 173(1), 636-667.

Cheng, M. & Heaton, T., 2013. Simulating building motions using the ratios of its natural frequencies and a Timoshenko beam model.. *Earthquake Spectra.*

Chopra, A., 2001. Dynamics of structures: theory and applications to earthquake engineering. 2nd ed. s.l.:Prentice-Hall.

Clough, R. & Penzien, J., 1975. *Dynamics of Structures*, McGraw-Hill.

Cowper, G., 1966. The shear coefficient in Timoshenko's beam theory. *ASME Journal of Applied Mechanics,* 33(2), 335-340.

FEMA (Federal Emergency Management Agency) (2005). *FEMA-440 Improvement of Nonlinear Static Seismic Analysis Procedures.* Federal Emergency Management Agency, Washington D.C.

Gazetas, G., 1983. Analysis of machine foundation vibrations: state of the art. *International Journal of Soil Dynamics and Earthquake Engineering,* 2(1), 2-42.

Ghahari, S., Abazarsa, F. & Taciroglu, E., 2015. *CSMIP-CIT.* V2.

Ghahari, S., Abazarsa, F., Ghannad, M. & Taciroglu, E., 2013. Response-only modal identification of structures using strong motion data. *Earthquake Engineering and Structural Dynamics,* 42(8), 1221-1242.

Ghahari, S., Abazarsa, F., Ghannad, M.A., Celebi, M. & Taciroglu, E., 2014. Blind modal identification of structures from spatially sparse seismic response signals. *Structural Control and Health Monitoring,* 21, 649-674.

Han, S., Benaroya, H. & Wei, T., 1999. Dynamics of transversely vibrating beams using four engineering theories.. Journal of Sound and Vibration, 225(5), 935-988.

Huang, M., & Shakal, A.F., 2001. Structural instrumentation in the California Strong Motion Instrumnetation Program. *Strong Motion Instrumentation for Civil Engineering Structures*, Springer Netherlands, 17-31.

IBC, 2012. *International Building Code,* Washington D.C: International Code Council.

Iguchi, M. & Luco, E., 1981. Dynamic response of flexible rectangular foundations on an elastic half-space. *Earthquake Engineering & Structural Dynamics,* 9(3), 239-249.

Ishibashi, I., & Zhang, X., 1993. Unified dynamic shear moduli and damping patios of sand and clay. *Soils and Foundations*, 33(1), 182-191.

Jennings, P. & Bielak, J., 1973. Dynamics of building-soil interaction. *Bulletin of the Seismological Society of America,* 63(1), 9-48.

Jennings, P. & Kuroiwa, J., 1968. Vibration and soil-structure interaction tests of a nine-story reinforced concrete building. *Bulletin of the Seism. Society of America*, 58(3), 891-916.

Kim, S., & Stewart, J.P., 2003. Kinematic Soil-Structure Interaction from Strong Motion Recordings. *Journal of Geotechnical and Geoenvironmental Engineering*, 129(4), 323-335.

Lignos, D. & Miranda, E., 2014. Estimation of base motion in instrumented steel buildings using output-only system identification. *Earthquake Engineering and Structural Dynamics*, 43(4), pp. 547-563.

Luco, J., Trifunac, M. & Wong, H., 1988. Isolation of soil-structure interaction effects by full-scale forced vibration tests. *Earthquake Engineering and Structural Dynamics,* 16(1), 1-21.

MATLAB, 2013. *MATLAB: The language of technical computing*., s.l.: Mathworks. The MathWorks Inc., Natick, MA.

NIST (National Institute of Standards and Technology), (2012). Soil-Structure Interaction for Building Structures, Report NIST/GCR 12-917-21, presented by NEHRP Consultants Joint Venture, J.P. Stewart (project director), September.

NEHRP, (1994). Recommended provisions for the developmement of seismic regulations for new buildings. Washington, D.C.: Building Seismic Safety Council.

NRC, (1995). *National Building Code of Canada.* Associate Committee on the National Building. Ottawa, Canada: National Research Council of Canada.

NRC/IRC, (2010). *National Building Code of Canada.* Ottawa, Ontario: National Research Council of Canada.

Pais, A. & Kausel, E., 1988. pproximate formulas for dynamic stiffnesses of rigid foundations.. *Soil Dynamics and Earthquake Engineering*, 7(4), 213-227.

Pak, R. & Guzina, B., 1999. Seismic soil-structure interaction analysis by direct boundary element methods. *International Journal of Solids and Structures,* 36(31), 4743-4766.

Pandit, S.M., 1991. Modal and Spectrum Analysis: Data Dependent Systems in State Space. Wiley-Interscience.

Richart, F., 1975. Some effects of dynamic soil properties on soil-structure interaction. *Journal of the Geotechnical Engineering Division (ASCE),* 101(2), 1193-1240.

Rizos, D. & Wang, Z., 2002. Coupled BEM–FEM solutions for direct time domain soil–structure interaction analysis. *Engineering Analysis with Boundary Elements,* 26(10), 877-888.

Seyhan, E., Stewart, J.P., Ancheta, T.D., Darragh, R.B., & Graves, R.W., 2014. NGA-West2 site database. *Earthquake Spectra*, 30(3), 1007-1024.

Snieder, R. & Safak, E., 2006. Extracting the building response using seismic interferometry: Theory and application to the Millikan Library in Pasadena, California. *Bulletin of the Seismological Society of America,* 96(2), 586-598.

Stewart, J., Seed, R. & Fenves, G., 1998. *Empirical evaluation of inertial soil-structure interaction effects*: Pacific Earthquake Engineering Research Center (PEER).

Stewart, J.P. 1996. An empirical assessment of soil-structure interaction effects on the seismic response of structures. Doctoral dissertation, University of California, Berkeley.

Stewart, J.P., & Stewart, A.F., 1997. Analysis of soil-structure interaction effects on building response from earthquake strong motion recordings at 58 sites. *Earthquake Engineering Research Center*, 97(1).

Stewart, J.P., Fenves, G.L., & Seed, R.B., 1999a. Seismic soil-structure interaction in buildings. I: Analytical methods. *Journal of Geotechnical and Geoenv. Eng.*, 125(1), 26-37.

Stewart, J.P., Seed, R.B., & Fenves, G.L., 1999b. Seismic soil-structure interaction in buildings. II: Empirical findings. *Journal of Geotechnical and Geoenv. Eng.*, 125(1), 38-48.

Taciroglu, E., Ghahari, S. & Abazarsa, F., 2016a. Efficient model updating of a multi-story frame and its foundation stiffmess from earthquake records using a Timoshenko beam model. *Soil Dynamics and Earthquake Engineering* (in print).

Taciroglu, E. & Ghahari, S., 2016b. Identification of Soil-Foundation Dynamic Stiffness from Seismic Response Signals. *ACI Special Publication* (in print).

Taciroglu, E., Ghahari, S. & Abazarsa, F., 2016c. Identification of soil-foundation-structure interaction effects using recorded strong motion response data from CSMIP-instrumneted buildings, UCLA-SGEL Report 2016-10.

Tileylioglu, S., Stewart, J. & Nigbor, R., 2010. Dynamic stiffness and damping of a shallow foundation from forced vibration of a field test structure. *Journal of Geotechnical and Geoenvironmental Engineering,* 137(4), 344-353.

Timoshenko, S., 1921. On the correction for shear of the differential equation for transverse vibrations of prismatic bars. *The London, Edinburgh, and Dublin Philosophical Magazine and Journal of Science,* 41(245), 744-746.

Todorovska, M., 2009. Soil-structure system identification of Millikan Library North–South response during four earthquakes (1970–2002): what caused the observed wandering of the system frequencies?. *Bulletin of the Seismological Society of America,* 99(2A), pp. 626-635.

UBC (Uniform Building Code), (1997). *International Conference of Building Officials.* Whittier, California.

Veletsos, A. & Verbic, B., 1973. Vibration of viscoelastic foundations. *Earthquake Engineering & Structural Dynamics,* 2(1), 87-102.

Veletsos, A.S., & Nair, V.V., 1975. Seismic interaction of structures on hysteretic foundations. *Journal of the Structural Division*, 101(1), 109-129.

Veletsos, A.S., Prasad, A.M., & Wu, W.H., 1997. Transfer functions for rigid rectangular foundations. *Earthquake engineering & structural dynamics*, 26(1), 5-17.

Wolf, J. & Deeks, A., 2004. Foundation Vibration analysis: A Strength of Materials Approach. Butterworth-Heinemann.

Wolf, J., 1976. Soil-structure interaction with separation of base mat from soil (lifting-off). *Nuclear Engineering and Design*, 38(2), 357-384.

Appendix A

Table A. List of candidate buildings for identification analyses.

No.	CSMIP	Floor No.*	NS	Type**	EW	Type**	Used Dir
1	58396	3	Y	MRSF	Y	MRSF	NS
2	13364	9	Y	MRSF	N	---	NS
3	58496	2	Y	BSF	Y	BSF	No
4	54388	2	Y	BSF	Y	MRSF	No
5	24370	6	N	---	Y	MRSF	EW
6	58661	3	Y	MRSF	Y	MRSF	No
7	24198	2	Y	MRSF	Y	MRSF	No
8	58466	4	Y	MRSF	Y	MRSF	No
9	58638	15	Y	Combined	Y	Combined	No
10	13214	5	Y	BSF	Y	BSF	No
11	14654	14	Y	BSF+MRSF	Y	BSF+MRSF	NS, EW
12	68032	3	N	---	Y	BSF+MRSF	No
13	57948	2	Y	Combined	N	---	No
14	57783	3	Y	Combined	N	---	No
15	13329	8	Y	Combined	Y	Combined	No
16	14533	15	Y	MRSF	Y	MRSF	EW
17	14323	7	Y	MRSF	Y	MRSF	EW
18	24581	14	Y	CSCF+UMW	Y	CSCF+UMW	No
19	24569	18	Y	MRSF+CSW	Y	MRSF+CSW	NS, EW
20	24643	23	Y	BSF	Y	MRSF	NS, EW
21	24332	5	Y	BSF	Y	BSF	NS
22	24288	32	Y	MRSF	Y	MRSF	NS
23	24602	52	Y	BSF+MRSF	Y	BSF+MRSF	EW
24	24629	58	Y	MRSF	N	---	No
25	24652	6	Y	BSF+MRSF	Y	BSF+MRSF	NS, EW
26	24713	8	Y	BSF	Y	BSF	No
27	31213	4	Y	Combined	N	---	No
28	57614	2	N	---	Y	BSF	No
29	12299	4	Y	MRSF	Y	MRSF	EW
30	24546	12	Y	MRSF	Y	MRSF	No
31	23481	8	Y	MRSF	N	---	NS
32	58506	3	Y	MRSF	Y	MRSF	No
33	23516	3	Y	MRSF	Y	MRSF	NS, EW
34	23515	9	Y	MRSF	Y	MRSF	NS, EW
35	03300	22	Y	MRSF	Y	MRSF	No
36	58776	15	Y	MRSF	Y	MRSF	No
37	58480	19	Y	MRSF	N	---	NS
38	58532	49	Y	MRSF	N	---	NS
39	57357	13	Y	MRSF	Y	MRSF	EW
40	57562	3	Y	MRSF	Y	MRSF	No
41	58261	4	N	---	Y	MRSF	EW
42	58593	3	N	---	Y	BSF	No
43	58199	4	N	---	Y	Combined	No
44	58506	3	Y	MRSF	Y	MRSF	NS, EW
45	24385	10	Y	CSW	Y	CSW	NS
46	58492	8	Y	CMSW	Y	CMSW	No
47	01260	6	N	---	Y	RCF	No
48	89494	5	N	---	Y	RMSW	No
49	58354	13	Y	MRSF+RCF+CSW	Y	MRSF+RCF+CSW	NS, EW
50	58488	4	N	---	Y	CSW	No
51	58462	7	Y	CSW	Y	CSW	NS, EW
52	12267	5	Y	CSW	Y	CSW	No
53	12493	5	Y	RCF+CSW	Y	RCF+CSW	NS

54	14311	5	Y	CSW	Y	CSW	EW
55	24236	14	Y	RCF	Y	RCF	NS, EW
56	24601	17	Y	CSW	Y	CSW	NS, EW
57	24463	6	Y	RCF	Y	RCF	NS, EW
58	24655	6	Y	CSW	Y	CSW	NS, EW
59	24231	7	N	---	Y	Combined	No
60	24468	9	Y	CSW	Y	CSW	NS, EW
61	57502	2	Y	CSW	Y	CSW	No
62	58641	8	N	---	Y	CSW	EW
63	13589	11	N	---	Y	CSW	EW
64	24464	22	Y	RCF	Y	RCF	NS, EW
65	58337	11	Y	CSW	Y	CSW	NS, EW
66	58639	13	Y	CSW	Y	CSW	NS, EW
67	58224	2	N	---	Y	CSW	No
68	58583	24	Y	CSW	Y	CSW	NS
69	12284	4	Y	CSW	Y	CSW	NS
70	24232	4	Y	CSW	Y	CSW	No
71	24454	4	Y	Combined	N	---	No
72	24571	11	Y	RCF	Y	RCF	NS, EW
73	58334	3	Y	CSW	Y	CSW	NS, EW
74	58348	3	N	---	Y	CSW	EW
75	23511	3	Y	RCF	Y	RCF	NS, EW
76	58503	4	Y	RCF+CSW	N	---	NS
77	13620	2	N	---	Y	CSW	No
78	23285	6	Y	CSW	Y	CSW	EW
79	23287	6	Y	CSW	Y	CSW	NS, EW
80	58490	6	Y	RCF	N	---	NS
81	03603	23	Y	Combined	Y	Combined	NS, EW
82	58437	47	Y	CSW	N	---	No
83	58411	58	Y	RCF+CSW	N	---	No
84	58479	6	Y	RCF+CSW	N	---	No
85	58389	64	N	---	Y	Combined	No
86	57355	11	Y	RCF	Y	CSW	NS, EW
87	57356	10	Y	CSW	Y	CSW	NS, EW
88	25213	3	Y	CSW	N	---	No
89	25302	4	Y	CSW	Y	CSW	NS, EW
90	48733	6	N	---	Y	RCF	EW
91	68489	14	Y	RCF+CSW	Y	RCF+CSW	NS, EW
92	68387	5	Y	CSW	Y	RCF	NS, EW
93	24322	15	Y	RCF	Y	RCF	NS, EW
94	24680	14	Y	CSW	Y	CSW	NS, EW
95	58055	4	Y	Combined	N	---	No
96	24514	6	Y	Combined	N	---	No
97	35409	3	Y	CSW	Y	CSW	NS
98	24386	7	Y	RCF	Y	RCF	NS, EW
99	25339	12	Y	CSW	Y	CSW	NS, EW
100	58364	10	Y	RCF+CSW	Y	RCF+CSW	NS, EW
101	47459	4	Y	CSW	Y	CSW	EW
102	14606	8	Y	RMSW	Y	RMSW	NS

* Counted floors above basement

** Moment Resisting Steel Frame (MRSF), Braced Steel Frame (BSF), Combination of several types along the height (Combined), Composite Steel-Concrete Frame (CSCF), Unreinforced Masonry Wall (UMW), Concrete Shear Wall (CSW), Concrete Masonry Shear Wall (CMSW), Reinforced Concrete Frame (RCF), Reinforced Masonry Shear Wall (RMSW)

Appendix B

Table B. Identified flexible base Timoshenko beam model's parameters (units are in SI).

No.	CSMIP No.	Dir	L (m)	D (m)	B (m)	Eq. Name	Eq. Year	$\bar{b}$	s	KR/M $(\times 10^3)$	KT/M $(\times 10^3)$
1	58354	EW	61.3	34.3	34.3	Loma Prieta	1989	0.373000	0.756800	R	R
2	58354	EW	61.3	34.3	34.3	Berkeley	2011	0.228900	1.250300	R	R
3	58354	NS	61.3	34.3	34.3	Loma Prieta	1989	0.445200	0.405780	118	R
4	58334	NS	22.3	22.0	35.0	San Leandro	2011	0.065380	0.117600	4159	13.992
5	58334	NS	22.3	22.0	35.0	Piedmont	2007	0.060000	0.313000	741	4.490
6	58334	NS	22.3	22.0	35.0	Berkeley	I 2011	0.061000	0.300000	1080	5.280
7	58334	EW	22.3	35.0	22.0	Loma Prieta	1989	0.048500	0.678300	R	13.648
8	58334	EW	22.3	35.0	22.0	Piedmont	2006	0.046900	0.713600	R	R
9	58334	EW	22.3	35.0	22.0	Lafayette	2007	0.047400	0.689400	R	R
10	58334	EW	22.3	35.0	22.0	Piedmont	2007	0.051000	0.632200	R	R
11	58334	EW	22.3	35.0	22.0	San Leandro	23 Aug. 2011	0.048200	0.622400	R	12.652
12	58334	EW	22.3	35.0	22.0	San Leandro	24 Aug. 2011	0.050000	0.561900	R	29.393
13	58334	EW	22.3	35.0	22.0	Berkeley	20 Oct. 2011 I	0.052400	0.658200	R	R
14	58334	EW	22.3	35.0	22.0	Berkeley	20 Oct. 2011 II	0.050800	0.663000	R	12.531
15	58334	EW	22.3	35.0	22.0	Elcerrito	2012	0.056100	0.513800	R	R
16	58334	EW	22.3	35.0	22.0	Piedmont	2015	0.053300	0.675200	R	R
17	24385	NS	26.8	22.9	66.6	Whittier	1987	0.173450	0.468120	R	R
18	24385	NS	26.8	22.9	66.6	Sierra Madre	1991	0.133020	0.761220	R	R
19	24322	NS	56.0	21.9	57.6	Encino	2014	0.075459	5.116600	R	R
20	24322	NS	56.0	21.9	57.6	Calexico	2010	0.058720	5.010800	R	R
21	24322	NS	56.0	21.9	57.6	Chinohills	2008	0.079708	4.769600	R	R
22	24322	NS	56.0	21.9	57.6	Chatsworth	2007	0.074253	4.826300	R	R
23	24322	EW	56.0	57.6	21.9	Landers	1992	0.310000	2.166000	R	R
24	24322	EW	56.0	57.6	21.9	Northridge	1994	0.941100	0.672700	R	R
25	24322	EW	56.0	57.6	21.9	Chinohills	2008	0.690800	0.215400	R	R
26	24322	EW	56.0	57.6	21.9	Calexico	2010	0.696300	0.198000	R	R
27	24322	EW	56.0	57.6	21.9	Encino	2014	0.644800	0.260100	R	R
28	58490	NS	23.8	27.4	61.0	Loma Prieta	1989	0.162500	1.404500	R	R
29	58462	EW	26.0	28.0	66.0	Alum Rock	2007	0.256210	0.329900	R	R
30	58462	EW	26.0	28.0	66.0	Loma Prieta	1989	0.262840	0.411820	R	R
31	58462	NS	26.0	66.0	28.0	Loma Prieta	1989	0.218700	0.754200	R	R
32	58462	NS	26.0	66.0	28.0	Lafayette	2007	0.128200	1.197400	R	R
33	58462	NS	26.0	66.0	28.0	Alum Rock	2007	0.137600	1.075300	R	R
34	0482	NS	60.0	50.5	50.5	Sierra Madre	1991	0.654010	0.670470	R	R
35	0482	NS	60.0	50.5	50.5	Big Bear	1992	0.694130	0.642560	R	R
36	13364	NS	38.1	35.4	66.5	Chinohills	2008	0.305530	1.221800	R	R
37	13364	NS	38.1	35.4	66.5	Lagunaniguel	2012	0.391860	0.706990	R	R
38	24370	EW	25.1	36.6	36.6	Northridge	1994	0.178130	1.875400	R	R
39	24370	EW	25.1	36.6	36.6	Sierra Madre	1991	0.179440	1.672900	R	R
40	24370	EW	25.1	36.6	36.6	Chatsworth	2007	0.140000	1.861200	R	R
41	24370	EW	25.1	36.6	36.6	Whittier	1987	0.176880	1.583600	49	R
42	24370	EW	25.1	36.6	36.6	Chinohills	2008	0.188670	1.643900	R	R
43	24370	EW	25.1	36.6	36.6	Whittier Narrows	2010	0.154820	1.688600	R	R
44	24370	EW	25.1	36.6	36.6	Calexico	2010	0.176070	1.656300	R	R
45	24370	EW	25.1	36.6	36.6	Borrego Springs	2010	0.173270	1.530800	R	R
46	23287	EW	15.6	17.7	52.5	Lomalinda	Feb. 2013	0.034318	0.747850	122	2.406
47	23287	NS	15.6	52.5	17.7	Landers	1992	0.117400	0.743600	R	1.444
48	23287	NS	15.6	52.5	17.7	Northridge	1994	0.122200	0.737300	R	2.062
49	23287	NS	15.6	52.5	17.7	Chinohills	2008	0.107000	0.747200	R	1.316
50	23287	NS	15.6	52.5	17.7	San Bernardino	2009	0.103700	0.833000	R	R
51	23287	NS	15.6	52.5	17.7	Borrego Springs	2010	0.117200	0.733800	R	9.116
52	23287	NS	15.6	52.5	17.7	Devore	2015	0.099400	0.877800	R	R
53	23287	NS	15.6	52.5	17.7	Banning	2016	0.101700	0.825400	R	R
54	14606	NS	23.0	19.0	65.0	Northridge	1994	0.137500	0.631000	56	R

55	14606	NS	23.0	19.0	65.0	Chinohills	2008	0.136430	0.552390	61	R
56	14606	NS	23.0	19.0	65.0	Calexico	2010	0.163700	0.416200	111	R
57	14606	NS	23.0	19.0	65.0	Borrego Springs	2010	0.152600	0.416200	98	R
58	14606	NS	23.0	19.0	65.0	Whittier Narrows	2010	0.127500	0.664100	91	R
59	58641	EW	24.0	10.7	15.0	Fremont	2015	0.287010	0.190180	R	R
60	58641	EW	24.0	10.7	15.0	Milpitas	2010	0.299880	0.145990	R	R
61	58641	EW	24.0	10.7	15.0	Alum Rock	2007	0.318730	0.155550	R	R
62	58641	EW	24.0	10.7	15.0	Gilroy	2002	0.296100	0.176670	R	R
63	58641	EW	24.0	10.7	15.0	Bolinas	1999	0.312050	0.146110	R	R
64	13589	EW	44.8	23.5	46.9	Landers	1992	0.331630	0.409200	R	R
65	13589	EW	44.8	23.5	46.9	Northridge	1994	0.353460	0.387770	R	R
66	13589	EW	44.8	23.5	46.9	Chinohills	2008	0.341250	0.390950	R	R
67	13589	EW	44.8	23.5	46.9	Inglewood	2009	0.302540	0.440660	R	R
68	13589	EW	44.8	23.5	46.9	Calexico	2010	0.322800	0.408370	R	0.259
69	13589	EW	44.8	23.5	46.9	Borrego Springs	2010	0.305860	0.408480	R	R
70	13589	EW	44.8	23.5	46.9	La Habra	2014	0.322800	0.408370	R	R
71	47459	EW	23.6	23.0	20.0	Morgan Hill	1984	0.065143	0.668250	203	1.692
72	47459	EW	23.6	23.0	20.0	Loma Prieta	1989	0.084400	0.636250	102	R
73	24386	NS	19.9	18.6	48.8	Westwood Village	2014	0.155830	0.324770	518	0.768
74	24386	NS	19.9	18.6	48.8	Encino	2014	0.130510	0.522700	135	1.016
75	24386	NS	19.9	18.6	48.8	Newhall	2011	0.146850	0.464940	R	0.805
76	24386	NS	19.9	18.6	48.8	Borrego Springs	2010	0.147080	0.464460	R	3.600
77	24386	EW	19.9	48.8	18.6	Big Bear	1992	0.224000	1.146700	R	0.113
78	24386	EW	19.9	48.8	18.6	Landers	1992	0.216500	1.187000	R	0.262
79	24386	EW	19.9	48.8	18.6	Northridge	1994	0.320400	1.315300	R	0.039
80	24386	EW	19.9	48.8	18.6	Chinohills	2008	0.088300	1.176300	R	1.039
81	24386	EW	19.9	48.8	18.6	Encino	2014	0.085800	1.254600	R	1.274
82	35409	NS	14.6	24.0	49.5	Maricopa	2010	0.074472	0.234860	R	1.734
83	35409	NS	14.6	24.0	49.5	Islavista	2013	0.074171	0.248940	R	2.238
84	58261	EW	16.0	35.7	66.8	South Napa	2014	0.142500	0.876280	R	R
85	58261	EW	16.0	35.7	66.8	Loma Prieta	1989	0.142500	0.876280	R	0.366
86	58261	EW	16.0	35.7	66.8	Morgan Hill	1984	0.136640	0.793480	R	R
87	24602	EW	236.0	48.0	48.0	Sierra Madre	1991	2.363900	0.436900	R	R
88	24602	EW	236.0	48.0	48.0	Northridge	1994	2.390100	0.453210	R	R
89	24602	EW	236.0	48.0	48.0	Landers	1992	2.536800	0.415460	R	R
90	24602	EW	236.0	48.0	48.0	Chinohills	2008	2.188100	0.485230	R	R
91	23515	NS	35.8	33.5	40.8	Landers	1992	0.749000	0.349500	20	R
92	23515	EW	35.8	40.8	33.5	Landers	1992	0.416000	1.123200	81	R
93	23516	NS	12.6	43.9	40.0	Landers	1992	0.057318	2.395300	R	R
94	23516	NS	12.6	43.9	40.0	Chinohills	2008	0.043297	2.710600	R	R
95	23516	NS	12.6	43.9	40.0	San Bernardino	2009	0.048140	2.730000	R	R
96	23516	EW	12.6	40.0	43.9	Whittier	1987	0.049300	2.351000	R	R
97	23516	EW	12.6	40.0	43.9	Landers	1992	0.058300	2.313500	R	R
98	23516	EW	12.6	40.0	43.9	Lake Elsinore	2007	0.074600	1.425300	R	R
99	23516	EW	12.6	40.0	43.9	Chinohills	2008	0.096800	1.086300	R	R
100	23516	EW	12.6	40.0	43.9	Inglewood	2009	0.077100	1.412500	R	R
101	23516	EW	12.6	40.0	43.9	San Bernardino	2009	0.109300	1.109100	R	R
102	23516	EW	12.6	40.0	43.9	Beaumont	2010	0.078700	1.337000	R	R
103	12284	NS	15.3	23.0	60.0	Palm Springs	1986	0.141900	0.122010	25	R
104	12284	NS	15.3	23.0	60.0	Borrego Springs	July 2010	0.163990	0.197210	14	R
105	12284	NS	15.3	23.0	60.0	Calexico	2010	0.161140	0.240760	21	R
106	12284	NS	15.3	23.0	60.0	Ocotillo	April 2010	0.153890	0.271970	22	R
107	57355	EW	43.0	25.0	58.0	Morgan Hill	1984	0.266940	0.354930	R	0.286
108	57355	EW	43.0	25.0	58.0	Loma Prieta	1989	0.317320	0.367170	R	0.232
109	57355	EW	43.0	25.0	58.0	Alum Rock	2007	0.270370	0.465510	R	R
110	57355	NS	43.0	58.0	25.0	Morgan Hill	1984	0.281000	0.680900	R	R
111	57355	NS	43.0	58.0	25.0	Loma Prieta	1989	0.400900	0.430200	R	0.302
112	57355	NS	43.0	58.0	25.0	Alum Rock	2007	0.425700	0.408600	R	0.221
113	57356	EW	29.0	19.0	64.0	Morgan Hill	1984	0.145360	0.095220	119	0.488
114	57356	EW	29.0	19.0	64.0	Loma Prieta	1989	0.155320	0.051201	120	0.257

115	57356	EW	29.0	19.0	64.0	Alum Rock	2007	0.149950	0.100200	122	0.440
116	57356	EW	29.0	19.0	64.0	Morgan Hill	2009	0.148940	0.102430	141	0.834
117	57356	EW	29.0	19.0	64.0	Milpitas	2010	0.152650	0.102080	148	0.465
118	57356	EW	29.0	19.0	64.0	Morgan Hill	2011	0.146340	0.124640	142	0.900
119	57356	EW	29.0	19.0	64.0	South Napa	2014	0.147100	0.152460	141	0.542
120	57356	NS	29.0	64.0	19.0	Morgan Hill	1984	0.136300	1.008800	R	0.419
121	57356	NS	29.0	64.0	19.0	Loma Prieta 1989	1989	0.163100	0.975900	R	0.243
122	57356	NS	29.0	64.0	19.0	Alum Rock	2007	0.146500	1.050300	R	0.559
123	58394	NS	32.0	26.0	59.0	Loma Prieta	1989	0.512280	0.102070	36	R
124	58394	EW	32.0	59.0	26.0	Loma Prieta	1989	0.321450	0.686960	R	0.187
125	58364	EW	39.0	32.0	45.0	Livermore	A 1980	0.249640	0.294790	134	0.670
126	58364	EW	39.0	32.0	45.0	Livermore	B 1980	0.240330	0.415720	119	0.402
127	58364	EW	39.0	32.0	45.0	Loma Prieta	1989	0.289130	0.305000	125	0.282
128	58364	EW	39.0	32.0	45.0	Alum Rock	2009	0.210800	0.485910	85	R
129	58364	EW	39.0	32.0	45.0	Alamo	2008	0.246970	0.378260	89	R
130	58364	EW	39.0	32.0	45.0	Berkeley	I 2011	0.204440	0.489100	92	R
131	58364	EW	39.0	32.0	45.0	Berkeley	II 2011	0.222730	0.434130	96	R
132	58364	EW	39.0	32.0	45.0	Elcerrito	2012	0.214210	0.460550	89	R
133	58364	EW	39.0	32.0	45.0	South Napa	2014	0.338600	0.191090	103	R
134	58364	EW	39.0	32.0	45.0	Concord	2015	0.236360	0.408170	90	R
135	58364	EW	39.0	32.0	45.0	San Ramon	2015	0.216010	0.485460	89	R
136	58364	NS	39.0	45.0	32.0	Alamo	2008	0.047018	2.998700	R	R
137	58364	NS	39.0	45.0	32.0	Berkeley	I 2011	0.041278	3.030000	R	R
138	58364	NS	39.0	45.0	32.0	Berkeley	II 2011	0.043805	2.902200	R	R
139	58503	NS	14.5	21.0	79.0	Loma Prieta	1989	0.115490	0.254130	R	1.075
140	58503	NS	14.5	21.0	79.0	Glen Ellen	2006	0.104480	0.248610	R	4.473
141	58503	NS	14.5	21.0	79.0	Berkeley	2011	0.092841	0.254050	R	1.332
142	58503	NS	14.5	21.0	79.0	Elcerrito	2012	0.101550	0.208170	R	0.933
143	58503	NS	14.5	21.0	79.0	South Napa	2014	0.099810	0.165940	R	1.156
144	58503	NS	14.5	21.0	79.0	Piedmont Area	2006	0.106270	0.227400	R	1.324
145	24601	EW	46.0	24.0	69.0	Sierra Madre	1991	0.430980	0.126910	141	R
146	24601	EW	46.0	24.0	69.0	Landers	1992	0.426300	0.128840	127	0.216
147	24601	EW	46.0	24.0	69.0	Northridge	1994	0.485470	0.105190	116	R
148	24601	NS	46.0	69.0	24.0	Sierra Madre	1991	0.332800	0.540080	R	R
149	24601	NS	46.0	69.0	24.0	Landers	1992	0.351930	0.533880	R	R
150	24601	NS	46.0	69.0	24.0	Northridge	1994	0.402050	0.500590	R	R
151	25339	EW	35.0	19.0	56.0	Santa Barbara	1978	0.251370	0.173230	R	R
152	25339	EW	35.0	19.0	56.0	Ojai	2013	0.253230	0.312970	R	R
153	25339	EW	35.0	19.0	56.0	Islavista	2013	0.237430	0.384810	R	R
154	25339	EW	35.0	19.0	56.0	Calexico	2010	0.224660	0.356860	R	R
155	25339	EW	35.0	19.0	56.0	Ojai	2009	0.248350	0.397600	R	R
156	25339	EW	35.0	19.0	56.0	Westlake Village	2009	0.244110	0.344760	R	R
157	25339	NS	35.0	56.0	19.0	Ojai	2013	0.289120	0.600678	R	0.388
158	24571	EW	39.6	25.9	64.9	Northridge	1994	0.285810	1.450100	16	R
159	24571	EW	39.6	25.9	64.9	Calexico	2010	0.221760	1.573600	22	0.071
160	24571	NS	39.6	64.9	25.9	Landers	1992	0.243800	1.259200	R	R
161	24571	NS	39.6	64.9	25.9	Northridge	1994	0.285200	1.057000	R	R
162	24571	NS	39.6	64.9	25.9	Whittier Narrows	2010	0.228900	1.055200	R	R
163	24571	NS	39.6	64.9	25.9	Calexico	2010	0.231100	1.071200	R	R
164	23285	EW	24.4	41.6	62.4	Fontana	2015	0.122500	0.949120	R	R
165	23285	EW	24.4	41.6	62.4	Big Bear Lake	2014	0.126430	0.902700	R	R
166	23285	EW	24.4	41.6	62.4	Fontana	2014	0.146840	0.781700	R	R
167	23285	EW	24.4	41.6	62.4	Borrego Springs	2010	0.175090	0.458690	R	R
168	23285	EW	24.4	41.6	62.4	Ocotillo	2010	0.168710	0.477330	R	R
169	23285	EW	24.4	41.6	62.4	Calexico	2010	0.172240	0.567160	R	2.018
170	24236	NS	45.3	15.5	66.1	Whittier	1987	0.832280	0.322260	R	0.052
171	24236	NS	45.3	15.5	66.1	Chinohills	2008	0.799350	0.341550	R	R
172	24236	NS	45.3	15.5	66.1	San Bernardino	2009	0.434890	0.687950	R	R
173	24236	EW	45.3	66.1	15.5	Whittier	1987	0.063994	2.339100	R	0.123
174	24236	EW	45.3	66.1	15.5	Chatsworth	2007	0.098390	1.353900	R	1.179

175	24236	EW	45.3	66.1	15.5	Chinohills	2008	0.129140	1.100100	R	0.905
176	24236	EW	45.3	66.1	15.5	San Bernardino	2009	0.180460	0.579650	R	2.078
177	24643	NS	96.0	33.5	92.3	Northridge	1994	1.849600	0.188000	R	R
178	24643	EW	96.0	92.3	33.5	Northridge	1994	1.407700	0.467100	R	R
179	12493	NS	24.2	25.8	54.9	Borrego Springs	June 2010	0.215060	0.535100	R	R
180	12493	NS	24.2	25.8	54.9	Borrego Springs	July 2010	0.261210	0.436760	R	R
181	12493	NS	24.2	25.8	54.9	Brawley	2012	0.243230	0.400000	R	R
182	12493	NS	24.2	25.8	54.9	Ocotillo	2010	0.222850	0.597760	R	R
183	12493	NS	24.2	25.8	54.9	Calexcio	2010	0.278700	0.400000	R	R
184	12493	NS	24.2	25.8	54.9	Chinohills	2008	0.227050	0.504420	R	R
185	24655	NS	18.0	69.0	82.0	Northridge	1994	0.098190	1.118400	R	0.724
186	24655	NS	18.0	69.0	82.0	Chinohills	2008	0.082608	1.215000	R	R
187	24655	NS	18.0	69.0	82.0	Calexico	2010	0.078879	1.148500	R	R
188	24655	NS	18.0	69.0	82.0	Borrego Springs	2010	0.077895	1.166400	R	R
189	24655	NS	18.0	69.0	82.0	Encino	2014	0.080010	1.201300	R	2.499
190	24655	NS	18.0	69.0	82.0	La Habra	2014	0.080815	1.217600	R	R
191	24655	EW	18.0	82.0	69.0	Northridge	1994	0.031000	2.202000	196	0.590
192	24655	EW	18.0	82.0	69.0	Chinohills	2008	0.033000	2.041000	250	0.440
193	24655	EW	18.0	82.0	69.0	Encino	2014	0.029000	2.121000	291	1.420
194	24655	EW	18.0	82.0	69.0	Lahabra	2014	0.029000	2.212000	284	R
195	68387	NS	20.0	20.0	38.0	South Napa	2014	0.132000	0.149000	120	0.570
196	68387	EW	20.0	38.0	20.0	South Napa	2014	0.216000	0.775700	R	R
197	58483	NS	66.7	23.8	64.0	Elcerrito	2012	0.874350	0.303160	R	R
198	58483	NS	66.7	23.8	64.0	Berkeley	20 Oct. 2011	0.925850	0.267540	R	R
199	58483	NS	66.7	23.8	64.0	Sanleandro	2011	0.853680	0.286530	R	R
200	58483	NS	66.7	23.8	64.0	Morgan Hill	2011	0.843520	0.303500	R	R
201	58483	NS	66.7	23.8	64.0	Alamo	2008	0.913800	0.237720	R	R
202	58483	NS	66.7	23.8	64.0	Piedmont	2007	0.891520	0.306230	R	R
203	58483	NS	66.7	23.8	64.0	Lafayette	2007	0.889700	0.285550	R	R
204	58483	NS	66.7	23.8	64.0	Loma Prieta	1989	1.286500	0.171560	R	R
205	58483	NS	66.7	23.8	64.0	South Napa	2014	0.820070	0.340070	R	R
206	58480	NS	73.3	29.3	21.3	Loma Prieta	1989	0.911830	0.466800	R	R
207	58480	NS	73.3	29.3	21.3	South Napa	2014	0.670200	0.576830	R	R
208	14654	NS	57.3	45.7	30.8	Northridge	1994	0.585900	0.481700	98	R
209	14654	NS	57.3	45.7	30.8	Chinohills	2008	0.571600	0.480100	126	R
210	14654	EW	57.3	30.8	45.7	Northridge	1994	0.931580	0.355070	R	R
211	14654	EW	57.3	30.8	45.7	Chinohills	2008	0.760490	0.476640	R	R
212	14654	EW	57.3	30.8	45.7	Inglewood	2009	0.617260	0.668900	R	R
213	14654	EW	57.3	30.8	45.7	Calexico	2010	0.801040	0.432330	R	R
214	14654	EW	57.3	30.8	45.7	Borrego Springs	2010	0.643060	0.557250	R	R
215	14654	EW	57.3	30.8	45.7	La Habra	2014	0.820970	0.400720	R	R
216	24680	NS	49.0	23.0	43.0	Chinohills	2008	0.587610	0.176880	372	R
217	24680	NS	49.0	23.0	43.0	Borrego Springs	2010	0.559940	0.173690	R	R
218	24680	NS	49.0	23.0	43.0	Encino	2014	0.619030	0.198100	R	R
219	24680	EW	49.0	43.0	23.0	Chinohills	2008	0.493400	0.284900	40	0.159
220	14323	EW	27.7	22.9	30.0	Whittier	1987	0.584960	0.309300	R	R
221	57318	EW	80.0	21.0	46.0	Alum Rock	2007	0.705280	0.274500	R	R
222	57318	EW	80.0	21.0	46.0	Morgan Hill	2011	0.526410	0.473160	R	R
223	57357	EW	50.0	45.0	45.0	Morgan Hill	1984	0.835500	0.381290	R	R
224	57357	EW	50.0	45.0	45.0	Loma Prieta	1989	0.708670	0.568850	R	R
225	57357	EW	50.0	45.0	45.0	Alum Rock	2007	0.591530	0.707190	R	R
226	57357	EW	50.0	45.0	45.0	Milpitas	2010	0.687010	0.430350	R	R
227	57357	EW	50.0	45.0	45.0	Morgan Hill	2011	0.589500	0.561710	R	R
228	58509	NS	55.0	40.0	55.0	South Napa	2014	0.299550	0.252450	R	R
229	58509	EW	55.0	55.0	40.0	South Napa	2014	0.447100	0.052300	R	R
230	24569	NS	75.6	105.0	48.0	Landers	1992	1.096400	0.488200	R	R
231	24569	EW	75.6	48.0	105.0	Landers	1992	1.099500	0.563100	R	R
232	24569	EW	75.6	48.0	105.0	Northridge	1994	1.102500	0.560850	R	R
233	58532	NS	180.0	37.0	55.0	Loma Prieta	1989	1.396700	0.860950	R	R
234	58532	NS	180.0	37.0	55.0	South Napa	2014	1.452500	0.763060	R	R

235	24463	NS	42.0	85.0	110.0	Whittier	1987	0.086482	4.075500	R	R
236	24463	NS	42.0	85.0	110.0	Northridge	1994	0.095949	4.118900	R	R
237	24463	NS	42.0	85.0	110.0	La Habra	2014	0.085610	3.947600	R	R
238	24463	NS	42.0	85.0	110.0	Encino	2014	0.079332	3.938600	R	R
239	24463	NS	42.0	85.0	110.0	Yorbalinda	2012	0.075694	3.930200	R	R
240	24463	EW	42.0	110.0	85.0	Whittier	1987	0.210300	1.533500	R	R
241	24463	EW	42.0	110.0	85.0	Borrego Springs	2010	0.223600	1.325000	R	R
242	24463	EW	42.0	110.0	85.0	Calexico	2010	0.224800	1.389800	R	R
243	24463	EW	42.0	110.0	85.0	Lahabra	2014	0.247900	1.212000	R	R
244	68489	EW	38.0	26.0	24.0	South Napa	2014	0.342160	0.445750	36	R
245	68489	NS	38.0	24.0	26.0	South Napa	2014	0.484780	0.249730	111	R
246	25302	NS	16.2	33.2	42.0	Santa Barbara	1978	0.087300	0.809400	R	R
247	25302	NS	16.2	33.2	42.0	Islavista	2013	0.087200	0.795300	R	R
248	25302	EW	16.2	42.0	33.2	Santa Barbara	1978	0.163600	0.743000	R	R
249	25302	EW	16.2	42.0	33.2	Islavista	2013	0.075900	1.173300	R	R
250	24288	NS	103.0	27.0	37.0	Chinohills	2008	0.542240	1.549900	R	R
251	24288	NS	103.0	27.0	37.0	Inglewood	2009	0.569940	1.318100	R	R
252	24288	NS	103.0	27.0	37.0	Whittier Narrows	2010	0.460980	1.558900	R	R
253	24288	NS	103.0	27.0	37.0	Calexico	2010	0.710160	1.107600	R	R
254	24288	NS	103.0	27.0	37.0	Borrego Springs	2010	0.693030	1.098800	R	R
255	24288	NS	103.0	27.0	37.0	Encino	2014	0.578820	1.297400	R	R
256	24288	NS	103.0	27.0	37.0	La Habra	2014	0.558770	1.397100	R	R
257	58348	EW	12.4	23.4	40.0	Loma Prieta	1989	0.076582	1.284900	R	R
258	58348	EW	12.4	23.4	40.0	Lafayette	2007	0.076582	1.284900	R	3.220
259	58348	EW	12.4	23.4	40.0	Piedmont	2007	0.072445	1.164200	R	3.019
260	58348	EW	12.4	23.4	40.0	Alum Rock	2007	0.069849	1.210100	R	1.061
261	58348	EW	12.4	23.4	40.0	Alamo	2008	0.069263	1.483700	R	0.892
262	58348	EW	12.4	23.4	40.0	Berkeley	20 Oct. 2011	0.074807	1.183800	R	2.241
263	58348	EW	12.4	23.4	40.0	Elcerrito	2012	0.069428	1.123510	R	R
264	58348	EW	12.4	23.4	40.0	South Napa	2014	0.079107	1.277900	R	3.926
265	58348	EW	12.4	23.4	40.0	San Ramon	2015	0.077098	1.097000	R	R
266	58348	EW	12.4	23.4	40.0	Concord	2015	0.077140	1.427400	R	R
267	14311	EW	21.6	22.8	62.0	Whittier	1987	0.116300	0.618600	R	R
268	14311	EW	21.6	22.8	62.0	Chinohills	2008	0.102100	0.652500	R	R
269	58639	EW	34.7	19.8	60.0	Bolinas	1999	0.225040	0.179640	172	1.305
270	58639	EW	34.7	19.8	60.0	Gilroy	2002	0.217940	0.175470	156	1.321
271	58639	EW	34.7	19.8	60.0	Piedmont	2007	0.227710	0.199650	182	R
272	58639	EW	34.7	19.8	60.0	Lafayette	2007	0.218131	0.334350	144	0.922
273	58639	EW	34.7	19.8	60.0	Alum Rock	2007	0.220450	0.198420	181	1.534
274	58639	EW	34.7	19.8	60.0	Elcerrito	2012	0.223320	0.200590	178	1.569
275	58639	EW	34.7	19.8	60.0	South Napa	2014	0.220490	0.207430	154	0.610
276	58639	NS	34.7	60.0	19.8	Bolinas	1999	0.234700	0.668710	R	0.571
277	58639	NS	34.7	60.0	19.8	Gilroy	2002	0.236090	0.633580	R	0.628
278	58639	NS	34.7	60.0	19.8	Piedmont	2007	0.244500	0.644810	R	0.214
279	58639	NS	34.7	60.0	19.8	Lafayette	2007	0.228480	0.650850	R	R
280	58639	NS	34.7	60.0	19.8	Alum Rock	2007	0.242070	0.646250	R	0.161
281	58639	NS	34.7	60.0	19.8	Elcerrito	2012	0.236660	0.636480	R	0.565
282	58639	NS	34.7	60.0	19.8	South Napa	2014	0.235470	0.682320	R	0.491
283	23511	EW	12.3	29.0	35.0	Whittier	1987	0.068497	0.888670	R	R
284	23511	EW	12.3	29.0	35.0	Chinohills	2008	0.095173	0.714250	R	R
285	23511	NS	12.3	35.0	29.0	Whittier	1987	0.061900	0.845400	R	R
286	23511	NS	12.3	35.0	29.0	Chinohills	2008	0.067200	0.851500	R	R
287	23511	NS	12.3	35.0	29.0	San Bernardino	2009	0.064200	0.745100	R	R
288	23511	NS	12.3	35.0	29.0	Whittier Narrows	2010	0.059800	0.887200	R	R
289	23511	NS	12.3	35.0	29.0	Borrego Springs	2010	0.063300	0.831100	R	R
290	23511	NS	12.3	35.0	29.0	Calexico	2010	0.061300	0.814800	R	R
291	23511	NS	12.3	35.0	29.0	Yorbalinda	June 2012	0.062800	0.831100	R	R
292	23511	NS	12.3	35.0	29.0	Yorbalinda	Aug. 2012	0.061200	0.834500	R	R
293	23511	NS	12.3	35.0	29.0	Pomona	2013	0.066300	0.830700	R	R
294	23511	NS	12.3	35.0	29.0	Anza	2013	0.061600	0.803100	R	R

295	14533	EW	81.0	32.0	32.0	Whittier	1987	0.782900	0.989600	R	R
296	14533	EW	81.0	32.0	32.0	Chinohills	2008	0.812300	0.987000	R	R
297	14533	EW	81.0	32.0	32.0	Inglewood	2009	0.750400	1.000600	R	R
298	14533	NS	81.0	32.0	32.0	Whittier	1987	0.778300	0.996500	R	R
299	24652	EW	26.0	29.0	29.0	Northridge	1994	0.385800	0.184100	354	R
300	24652	EW	26.0	29.0	29.0	West Hollywood	2001	0.259200	0.394500	50	R
301	24652	EW	26.0	29.0	29.0	Chinohills	2008	0.340300	0.232500	R	R
302	24652	EW	26.0	29.0	29.0	Inglewood	2009	0.343700	0.205830	52	R
303	24652	NS	26.0	29.0	29.0	Northridge	1994	0.324300	0.269000	72	0.339
304	24652	NS	26.0	29.0	29.0	West Hollywood	2001	0.205200	0.584600	47	R
305	24652	NS	26.0	29.0	29.0	Chinohills	2008	0.309400	0.280400	78	R
306	24652	NS	26.0	29.0	29.0	Inglewood	2009	0.286200	0.306700	73	R
307	24464	NS	54.0	17.4	56.0	Northridge	1994	0.996560	0.526630	R	R
308	24464	NS	54.0	17.4	56.0	Chinohills	2008	0.609050	0.766780	R	R
309	24464	EW	54.0	56.0	17.4	Whittier	1987	0.838000	0.301500	R	R
310	24464	EW	54.0	56.0	17.4	Northridge	1994	0.618200	0.920500	R	R
311	24464	EW	54.0	56.0	17.4	Chinohills	2008	0.458700	0.981300	R	R
312	24464	EW	54.0	56.0	17.4	Calexico	2010	0.476100	0.914100	R	R
313	58337	EW	35.0	21.0	60.0	Morgan Hill	2011	0.184400	0.332370	255	0.603
314	58337	EW	35.0	21.0	60.0	Sanleandro	24 Aug. 2011	0.120370	0.682870	167	0.981
315	58337	EW	35.0	21.0	60.0	Sanleandro	23 Aug. 2011	0.114680	0.696590	204	0.830
316	58337	EW	35.0	21.0	60.0	Berkeley	I 2011	0.163390	0.477520	153	R
317	58337	EW	35.0	21.0	60.0	Berkeley	II 2011	0.135490	0.640120	147	R
318	58337	EW	35.0	21.0	60.0	Berkeley	27 Oct. 2011	0.116090	0.720360	225	R
319	58337	EW	35.0	21.0	60.0	Elcerrito	2012	0.143550	0.523910	185	R
320	58337	NS	35.0	60.0	21.0	Elcerrito	2012	0.042915	2.947000	R	1.907
321	58337	NS	35.0	60.0	21.0	Berkeley	27 Oct. 2011	0.052010	2.332800	R	R
322	58337	NS	35.0	60.0	21.0	Berkeley	II 2011	0.044991	2.820000	R	0.762
323	58337	NS	35.0	60.0	21.0	Berkeley	I 2011	0.044436	2.883500	R	0.678
324	58337	NS	35.0	60.0	21.0	Sanleandro	24 Aug. 2011	0.045374	2.606100	R	1.126
325	58337	NS	35.0	60.0	21.0	Sanleandro	23 Aug. 2011	0.043691	2.884400	R	2.519
326	58337	NS	35.0	60.0	21.0	Morgan Hill	2011	0.041933	2.771200	R	1.196
327	58336	EW	48.8	40.0	40.0	Berkeley	2011	0.345600	0.445000	278	0.428
328	58336	EW	48.8	40.0	40.0	South Napa	2014	0.322900	0.516100	114	R
329	58336	EW	48.8	40.0	40.0	Piedmont	2015	0.202700	0.974600	151	R
330	48733	EW	24.0	56.0	56.0	Gilroy	2002	0.102090	1.590000	R	R
331	48733	EW	24.0	56.0	56.0	Parkfield	2004	0.108620	1.549300	R	R
332	48733	EW	24.0	56.0	56.0	Alum Rock	2007	0.120200	1.526800	R	R
333	12299	EW	16.0	24.0	45.0	Hector Mine	1999	0.048214	3.181200	R	R
334	12299	EW	16.0	24.0	45.0	Palm Springs	1986	0.074328	2.112300	R	0.214
335	12299	EW	16.0	24.0	45.0	Borrego Springs	2010	0.053447	2.853600	R	0.598
336	23481	NS	27.4	28.3	42.7	Landers	1992	0.633290	0.299130	R	R
337	23481	NS	27.4	28.3	42.7	Calexico	2010	0.721940	0.287750	R	R
338	23481	NS	27.4	28.3	42.7	Borrego Springs	2010	0.700760	0.276930	R	R
339	23481	NS	27.4	28.3	42.7	Redlands	2010	0.567700	0.301400	R	R
340	58615	EW	68.7	30.5	68.6	Alum Rock	2007	0.681950	0.485660	109	R
341	58615	EW	68.7	30.5	68.6	Glen Ellen	2006	0.632880	0.546400	205	R
342	58615	EW	68.7	30.5	68.6	Gilroy	2002	0.607730	0.576290	128	R
343	58615	EW	68.7	30.5	68.6	South Napa	2014	0.664750	0.511150	237	R
344	03603	NS	95.0	26.0	58.5	Chinohills	2008	0.918270	0.476890	R	R
345	03603	NS	95.0	26.0	58.5	San Clementels	2004	0.946850	0.467980	R	R
346	03603	NS	95.0	26.0	58.5	Borrego Springs	2010	1.087300	0.387490	R	R
347	03603	NS	95.0	26.0	58.5	Calexico	2010	1.133600	0.368200	R	R
348	03603	EW	95.0	58.5	26.0	Chinohills	2008	1.258100	0.285110	R	R
349	03603	EW	95.0	58.5	26.0	San Clementels	2004	1.161300	0.346080	R	R
350	03603	EW	95.0	58.5	26.0	Borrego Springs	2010	1.324500	0.287690	R	R
351	03603	EW	95.0	58.5	26.0	Calexcio	2010	1.392800	0.255690	R	R
352	24468	NS	38.7	19.2	46.9	La Habra	2014	0.523910	0.442350	R	R
353	24468	NS	38.7	19.2	46.9	Chinohills	2008	0.583840	0.339320	R	R
354	24468	NS	38.7	19.2	46.9	Northridge	1994	0.563620	0.533990	R	R

355	24468	NS	38.7	19.2	46.9	Yorbalinda	2012	0.367500	0.721810	R	R
356	24468	EW	38.7	46.9	19.2	Whittier	1987	0.295400	1.255500	R	R
357	24468	EW	38.7	46.9	19.2	Northridge	1994	0.281500	1.245500	R	R
358	58196	EW	17.0	31.0	79.0	Berkeley	2011	0.028196	1.589600	88	5.026
359	58196	EW	17.0	31.0	79.0	Morgan Hill	2011	0.035090	1.327000	105	2.121
360	58196	EW	17.0	31.0	79.0	Piedmont	2007	0.044912	1.007300	94	2.649
361	58196	EW	17.0	31.0	79.0	Lafayette	2007	0.031119	1.543400	86	R
362	58196	EW	17.0	31.0	79.0	Alamo	2008	0.033245	1.314200	93	R
363	05407	NS	44.0	21.0	23.0	Yorbalinda	2002	0.234000	0.269000	351	R
364	05407	NS	44.0	21.0	23.0	San Simeon	2003	0.208000	0.392000	239	0.320
365	24332	NS	22.1	66.7	73.0	Whittier	1987	0.107800	0.714200	R	0.483
366	24332	NS	22.1	66.7	73.0	Northridge	1994	0.072100	1.971200	R	R
367	24332	NS	22.1	66.7	73.0	Encino	2014	0.063400	1.843900	R	R
368	58396	NS	12.5	38.1	45.7	Berkeley	2011	0.051000	1.511000	R	R
369	58396	NS	12.5	38.1	45.7	South Napa	2014	0.080900	0.895300	R	R
370	58396	NS	12.5	38.1	45.7	Concord	2015	0.047300	1.628400	R	R
371	58396	NS	12.5	38.1	45.7	Piedmont	2015	0.052600	1.590600	R	R
372	58506	EW	14.0	24.0	50.0	Loma Prieta	1989	0.235800	0.469200	151	0.288
373	58506	NS	14.0	50.0	24.0	Loma Prieta	1989	0.045800	3.257000	R	R